Front wall and in-chamber impact loads on a breakwater-integrated oscillating water column

Front Wall and In-Chamber Impact Loads in an Oscillating Water Column Integrated Vertical Breakwater

Krisna A. Pawitan[a*], Diego Vicinanza[b], William Allsop[c], Tom Bruce[d]

a *School of Engineering, The University of Edinburgh, King's Buildings, Edinburgh EH9 3JL, United Kingdom. k.pawitan@ed.ac.uk*

b *Department of Engineering, University of Campania "Luigi Vanvitelli", via Roma 9, 81031 Aversa (CE), Italy. diego.vicinanza@unicampania.it*

c *William Allsop Consulting Ltd., The White House Denchworth Road, Grove, Wantage, Oxon, England, OX12 0AR, United Kingdom. william.allsop51@outlook.com*

d *School of Engineering, The University of Edinburgh, King's Buildings, Edinburgh EH9 3JL, United Kingdom. Tom.Bruce@ed.ac.uk*

**corresponding author*

Abstract

Large-scale tests (about 1:9 of full scale) were carried out at the Large Wave Channel (GWK) on Oscillating Water Column (OWC) wave energy converters to analyse loading and water column behaviour over a wide range of wave steepnesses. The paper shows that prediction methods for non-impulsive wave loads and impulsive wave loads developed for conventional vertical breakwaters can be adapted for OWCs with an adjustment factor (λ). The wave load analysis demonstrates that the impact probability method from project Probabilistic Design Tools for Vertical Breakwater (PROVERBS) estimates well the proportion of impacts experienced. Observations within the OWC chamber provide new insight on water column behaviour, including three different classifications of impacts during operation: "single impact", "successional impact", and "water column impact". These identify wave conditions at risk of violent impact inside the chamber.

Keywords: impact loads, impulsive loads, Oscillating Water Column installed Vertical Breakwater, water column behaviour

Introduction

Generally, a breakwater is only used to provide shelter for the harbour. The integration of energy dissipating wave chambers into a breakwater design, however, opens the possibility of an Oscillating Water Column (OWC) – Wave Energy Converter (WEC) to be integrated

within a breakwater caisson (Vicinanza *et al.,* 2019; He and Huang, 2016; Jarlan, 1961; Takahashi *et al.,* 1986; Takahashi, 1988). This idea was successfully implemented by a combined wave energy power plant and breakwater in the port of Mutriku, Spain. This concept allows the cost to be split between the harbour protection and energy generation function of the structure. Although now operating, the power plant construction was not a smooth process, suffering severe storm damage in December 2007, March 2008, and January 2009. These storms caused 4 of the 16 chambers to be severely damaged, including the loss of the entire section of the front wall as shown in Figure 1 (a) and (b) (Horvath, 2009). A subsequent study suggests that the pressure experienced by the structure may have reached 6 times the 'operational' limits of the walls during these storms (Medina-Lopez *et al.,* 2015). These conditions highlight the design uncertainties in an OWC installed breakwater design when exposed to actual wave loads, especially impact loads. There has been a century of quantified observation on wave loadings occur on a breakwater (Viviano *et al.,* 2019; Lugni *et al.,* 2010a; Lugni *et al.*, 2010b; Lugni *et al.,* 2006; Oumeraci et al., 2001) including the one caused by overtopped bore, such as during the event like tsunami (Streicher *et al.,* 2017, Streicher *et al.,* 2018 and Streicher *et al.,* 2019). The earlier attempt to model the wave loads ignored the distinction between a non-impulsive and impulsive wave loads (Hiroi, 1919). A newer model, however, was developed to estimate the non-impulsive wave loads prediction (Sainflou, 1928; Goda 1975; 2010).

Unlike non-impulsive wave loads, impulsive loads, which often come from breaking waves, have an unpredictable nature and much higher local pressures (Kirkgöz, 1995; Allsop *et al.,* 1996a; Laju *et al.,* 2005; Bullock *et al.*, 2007; Kisacik *et al.*, 2012; Hattori *et al.,* 1994; Topliss *et al.,* 1993). Several failures have shown that impact pressure may cause catastrophic structural damage to a breakwater (Oumeraci, 1994; Oumeraci *et al.,* 1993). Building on an

original concept introduced by Hiroi (1919), Bagnold (1939) later introduced 'Bagnold number', or B_a, to predict the maximum impact pressure (Equation 1).

$$B_a = \left(\frac{\rho_w k_{Ba} u_0^2}{p_o D_{Ba}}\right) \quad (1)$$

with ρ_w denotes water density, k_{Ba} denotes the effective height of water mass, u_o denotes the water mass impinging velocity, p_o denotes the atmospheric pressure, and D_{Ba} denotes the air pocket thickness. For vertical breakwater, Mitsuyasu (1961) and Cuomo *et al.,* (2010b) show that the u_o, D_{Ba}, and k_{Ba} can be approximated with Equations 2, 3, and 4, respectively.

$$(u_o = \sqrt{g(d + H_{m0})}) \quad (2)$$

$$(D_{Ba} = \frac{\pi}{12} H_{m0}) \quad (3)$$

and

$$(k_{Ba} = 0.2\left(1 - \frac{\pi}{12}\right) H_{m0}) \quad (4)$$

A semi-empirical relationship between the impact rise time (t_r) and the impact force magnitude (F_i) later introduced as Equation 5.

$$F_{imp} = a.t_r^b \quad (5)$$

where a and b are empirical constants chosen to include all of the experimental impact force measurements scatter by Weggel and Maxwell, 1970. Subsequent work showed that for a conventional vertical breakwater, the impact force (F_{imp}) should not exceed the equation with a and b listed Table 1 depending on the non-exceedance level (Cuomo *et al.,* 2010a; Cuomo *et al.,* 2011).

McKenna and Allsop (1996b) suggested that the transition point between the non-impulsive wave loads and impulsive wave loads in an irregular wave train can be seen in a change of

gradient in a non-exceedance probability distribution of the front wall force. The Probabilistic Design Tools for Vertical Breakwater (PROVERBS) project (Oumeraci *et al.,* 2001) also established a design guidance to estimate the percentage of impacts that may occurs in an irregular wave train and was intended as a design tools for breakwaters.

In addition to the wave loads occurring on the front wall, recent findings suggest that in-chamber impact occur inside an OWC chamber during operation (Müller and Whittaker, 1993; Müller and Whittaker, 1995; Takahashi *et al.,* 1985).

This paper will use data from large-scale tests to explore and quantify impact loads on, and inside an OWC caisson. Furthermore, the results will be compared with the existing method developed exclusively for conventional vertical breakwater. In addition, the wave conditions under which chaotic water volume behaviour occurs will be mapped by means of in-chamber video recording for both Regular and Irregular wave conditions.

The large-scale model employed for the experiments is introduced in Chapter 2. The discussion then will be done for both the front wall (Chapters 3, 4, and 5) and the OWC caisson (Chapters 6 and 7). The details are as follow: The wave loadings experienced by the front wall are explored for both non-impulsive loads (Chapter 3) and impulsive loads (Chapter 4). The comparison between the predicted number of impacts in an irregular wave train and the experiments will be provided in Chapter 5. The in-chamber ceiling impacts are characterised, classified, and quantified in Chapter 6, while the wave conditions which could result in a risk of in-chamber impacts are mapped in Chapter 7. Finally, conclusions are drawn in Chapter 8.

Methodology

A physical model utilisation for impulsive wave loads observation on coastal structure has been proven to be critical because numerical modelling, at the current state, won't be able to

98 simulate the complex interaction between water and air correctly (Hughes, 2014). In this
99 paper, a large-scale physical model tests have been done in the large wave channel (Grosse
100 Wellenkanal, GWK) in Hannover, Germany. The tests were carried out in a 307m long, 5m
101 wide, and 7m deep wave flume, with significant wave heights (H_{m0}) from 0.26m to 0.81m
102 and peak wave period from 3s to 6.5s. The large-scale model is a 1:9 scale to the prototype
103 with structure loosely based on the Mutriku OWC installed vertical breakwater and the then
104 proposed OWC device at Siadar, Isle of Lewis, Scotland (Patterson *et al.,* 2010). Figure 2
105 shows the schematic of the large-scale physical model used in the experiments. It is important
106 to note that qualitative observation and measured pressure signals analysis shows no evidence
107 of the structure's oscillation under impact pressure, indicating frequencies higher than the
108 sampling frequency. Because of this, it is safe to say that the structure is rigid enough for the
109 impact experiments. To measure the wave pressure experienced by the front wall, a line of
110 five pressure transducers were placed vertically on the front wall (P1-P5) and the in-chamber
111 rear wall (P8 – P12). Two pressure sensors were also placed on the front part (P6) and rear
112 part (P7) of the ceiling. The recording duration was done for at least 1000 wave cycle for
113 each wave condition, so it varies depending on the significant wave condition. The sampling
114 rate is limited to 1000 Hz for all cases. The pressure transducer used for the experiment are
115 the General Electric Druck Sensing type PDCR 1830 pressure sensor. This type of pressure
116 sensor has the maximum pressure measurement of 7.5kPa with measuring frequency above
117 the recording frequency. All of the pressure sensors were calibrated every day. It is safe to
118 say that the sensor measurement results are trustworthy. Apart of the sensor errors, it is
119 possible for a minimum amount of air trapped between the impinging water mass and the
120 sensor membrane. The front wall of the physical model has a 1m height opening, which
121 connected the water column inside the chamber and the outer sea. The still water level (swl)

122 located 1.8m from the bottom of the structure, giving an air chamber height of 0.7m inside
123 the OWC.

124 To simulate the power take-off mechanism of an OWC device, an interchangeable orifice
125 opening was mounted 1.4m above the chamber ceiling, in a 0.5m diameter 'chimney' located
126 on the centre of the ceiling. Figure 3 shows the photo of the structure during the experiment
127 with a breaking wave impacting the front wall. There are three identical chambers side by
128 side used during the experiment, but only the centre structure is instrumented. The other two
129 chambers were installed with the same PTO arrangement and setting to ensure that they are
130 hydraulically identical. For more detail on the experimental set-up, please see Pawitan *et al.,*
131 (2019) and Viviano *et al.,* (2016).

132 Five different orifice:chamber area ratios (A_o/A_c) were used to vary the damping
133 characteristics inside the chamber: 0.0% (closed), 0.1%, 0.2%, 0.88%, and 2.0% which
134 offered very little resistance to the air flow. Furthermore, a video camera is installed inside
135 the chamber, on the front part of the ceiling, facing the in-chamber rear wall, to enable visual
136 study of the in-chamber water movement with recording frame rate of 30 frame per second. It
137 is understood that the water column impact may move faster than the frame rate available, but
138 the video recording was intended as qualitative observation only to give early indication of
139 impact(s) occurrence.

140 Figure 4 and Table 2 shows the irregular wave conditions tested in the experiments. These
141 wave conditions were selected to cover a wide range of wave steepnesses within the
142 limitations of the wave generator's capability. The irregular waves were generated using
143 JONSWAP spectrum with peak enhancement factor (γ) of 3.3. A single wave sequence is
144 determined using zero-up crossing method of a wave gauge measurement located 1m in front

of the structure. It is important to understand that the maximum impact pressure occurs locally and may not occur exactly at the pressure transducer's location.

To calculate the impact force magnitude, a centred rectangular pressure integration method is employed. This method estimates the instantaneous magnitude of force experienced by the wall (either the front wall, rear wall, or ceiling) by assuming the pressure measured at certain PT location represents the pressure over associated area. The interval used to calculate the associated area can be seen in Figure 5. The measured force (F_{meas}) is calculated using

$$F_{meas} = \sum_{n=1}^{N} F_n = \sum_{n=1}^{N} (X_n - X_{n-1}) p_n \qquad (6)$$

where p_n denotes the pressure measured at the location X_n. In this experiment, N is equal to 5 for both front and rear wall, and 2 for the ceiling. Front wall higher than X_5 is not considered for the force calculation, while for the rear wall X_5 is equal to the chamber ceiling height.

Front wall - non-impulsive loads

Adding an OWC chamber into a vertical breakwater is anticipated to affect the wave loads experienced by the front wall of the structure. Established prediction methods, however, solely focused on a conventional breakwater. Figure 6 (a) – (c) show the comparison between the measurements for closed orifice (circle), A_o/A_c = 0.1% (square), 0.2% (diamond), 0.88% (triangle), and 2.0% (star); and the Goda prediction method (solid line) (Goda, 2010). The measured pressure plotted is defined as the mean of the largest 1/250th of individual wave event pressure maxima. Here, because the irregular wave trains were 1000 T_p in length (so normally 1000-wave sequences), this $P_{1/250}$ measure is selected because it should be representative of the largest pressure maxima, but less susceptible to scatter than a simple P_{max} measure.

The irregular wave conditions are (a) H_{m0} = 0.26m and T_p = 3s (Irr01), (b) H_{m0} = 0.39m and T_p = 3s (Irr02), and (c) H_{m0} = 0.26m and T_p = 4.5s (Irr13). The Goda prediction is only shown

169 down to an elevation of -0.7m because that is the end of the front wall penetration. As can be
170 seen from the figure, the Goda prediction method gives a safe prediction for all of the cases
171 including the closed orifice. Due to the limitation to time, only the 0.88% case was tested for
172 figure (b). The trend, however, remains the same for all of cases with all data points located
173 below the prediction line. It appears, therefore, that Goda prediction method gives a
174 conservative prediction of the front wall pressure distribution in the OWC installed
175 breakwater case under non-impulsive conditions.

176 **Front wall – impulsive loads**

177 Allsop *et al.* (1996a) and Oumeraci (1994) characterised three types of impact pressure
178 experienced by the front wall based upon the rise time (t_r), defined as the time between the
179 start of an impact event and the occurrence of the force maximum of the impact. The time
180 from the impact's start to the transition point where the pressure signal looks more similar to
181 a non-impulsive wave loads is called the duration (t_d). The first type (Figure 7) is a *severe*
182 *impact* pressure on the vertical wall which characterised by a short rise time ($t_r \sim 0.01T_p$) and
183 the highest-pressure peaks. The second type is a *less severe impact* pressure with smaller
184 pressure maximum and a second smaller peak after the impact (Figure 8). The rise (t_r) for this
185 type is longer than the first type ($t_r \sim 0.1T_p$). The final type characterised is a *double peaked*
186 pressure resulted from steep near-breaking waves with more obvious double pressure peaks
187 and of similar magnitude (Figure 9) and longer rise time ($t_r \approx 0.2T_p$). Figure 10 illustrates the
188 definitions of rise time (t_r), duration (t_d), and maximum impact pressure measured ($p_{i,max}$) of
189 Figure 7.

190 To explore the relationship between the impact force (F_{imp}) and the rise time (t_r), the
191 normalised measured force is plotted against the associated normalised rise time in Figure 11.
192 The normalisation is done by dividing the measured impact force with the average of four
193 biggest non-impulsive force of the same irregular wave train ($F_{imp}/F_{ni,1/250}$) and the rise time

194 with the peak wave period (t_r/T_p). The line presented is the relationship proposed by Cuomo
195 et al. (2011) at various non-exceedance level (Table 1). The top line is the 99.9% non-
196 exceedance level with 25% relative error line. As can be seen from the figure, the F_{imp} and t_r
197 relationship for the OWC installed vertical breakwater also follows Equation 1. Some of the
198 data points are still located above the higher error prediction line. This can be caused by the
199 fact that, unlike a conventional breakwater, the OWC installed breakwater has an opening on
200 the front wall. This condition makes the incident wave below certain elevation continue to
201 flow into the chamber, which may cause a higher impact rise time (t_r).

202 Since these experiments utilised a scale physical model, the impact pressure measured may
203 not scaled up correctly with Froude scaling which ignore the fluid flow characteristics
204 similarity between the model and the prototype (Hughes, 1993) . Takahashi (1985) proposed
205 an adjustment factor (λ) (Equation 7) of 3.01 to be used for scale model wave loads analysis,
206 in order to compensate for the uncertainty associated with impact loads in physical model
207 testing.

208 $$\lambda = \frac{(p_{max})_m \cdot s_c^{-1}}{(p_{max})_p} \qquad (7)$$

209 where $(p_{max})_m$ denotes the maximum impact pressure measured in the scale-model, $(p_{max})_p$
210 denotes the predicted maximum impact pressure at the prototype scale by utilising Bagnold
211 number (B_a), and s_c denotes the scale ratio between the model and the prototype. This
212 adjustment factor later extended to include multiple different scales by Cuomo *et al.* (2010b).

213 The same method is used in the current paper to find the adjustment factor (λ) for the large-
214 scale test results. For example, for the Irr11 wave conditions, the significant wave height
215 (H_{m0}) is 1.00m, so the Bagnold number of the model is equal to 0.153. Since the large-scale
216 model is about 1:9 to the prototype, the Bagnold number of the prototype will be 1.378, thus
217 $(p_{i,max})_p$ is 377 kPa. The experimental results of Irr11 (Figure 12) show the impact pressure

measured $(p_{i,max})_m$ is 223 kPa, so the model is over-estimating the prototype impact pressure by a factor (λ) of 5.34, which very much inline with Cuomo *et al.* (2010b). It is important to remember that an impact load occurs locally, and its maximum may not occur exactly at the pressure transducer location during the experiment.

Front wall – Probability of impacts ($P_{i\%}$)

A simple method to estimate the percentage of impacts in a single irregular wave train on a vertical breakwater was developed by Calabrese and Vicinanza (1999) as part of the Probabilistic Design Tools for Vertical Breakwater (PROVERBS) project (Oumeraci *et al.*, 2001). The estimation depends upon the water depth offshore of the structure (h) and the depth of the water just in front of the front wall, which in this case equal to the in-chamber water depth (d). The method uses a calculation the breaking wave height (H_{bc}) to predict the state of each incident wave when it hits the structure - whether it be in the condition of non-breaking (more likely to give a non-impulsive wave loads), near breaking and breaking (impact loads) or broken (non-impulsive wave loads). The wave height at breaking is given by Equation 8

$$H_{bc} = (0.1025 + 0.0217\ C^*)\ L_{pi}\ tanh\left(2\pi\ k_b h/L_{pi}\right) \qquad (8)$$

where L_{pi} and C^* can be calculated using Equations 9 and 10 respectively.

$$L_{pi} = \left(gT_p^2/2\pi\right)\ tanh\left(2\pi\ h/L_{pi}\right) \qquad (9)$$

and

$$C^* = (1 - C_r)/(1 + C_r) \qquad (10)$$

where k_b is the empirical berm constant and equal to 1 when no berm is present, L_{pi} is the wavelength associated with the peak period in the water depth h, C^* is a reflection measure depending upon the overall reflection coefficient C_r, and H_{bc} is the wave height at breaking.

Table 3 lists the reflection coefficient of each experimental test after Viviano *et al*. (2016), with method based upon Faraci *et al.,* (2014) four probes method.

To give the maximum possible percentage of impact, the percentage of waves which passed the non-breaking-to-breaking point (P_b) has to be estimated using Equation 11 with H_{si} denoting the incident wave height and H_{bc} denoting the breaking wave height.

$$P_b = \exp[-2\left(\frac{H_{bc}}{H_{si}}\right)] \quad (11)$$

The breaking to broken transition wave height (H_{bs}) can be estimated using Equation 12.

$$H_{bs} = 0.1242\, L_{pi}\, tanh\left(2\pi\, h_s/L_{pi}\right) \quad (12)$$

Thus, the percentage of impacts can be calculated by subtracting the number of broken waves in P_b according to Equation 13.

$$P_{i\%} = \left\{exp\left[-2\left(\frac{H_{bc}}{H_{si}}\right)^2\right] - exp\left[-2\left(\frac{H_{bs}}{H_{si}}\right)^2\right]\right\}.100\% \quad (13)$$

To compare the $P_{i\%}$ estimations with the experiment, the rectangular force calculation is applied for the front wall, based on pressure transducers P1-P5 measurements. The percentage of impact is estimated for 1000 wave cycles for each irregular condition. Figure 13 shows the plotted comparison between the estimation (circle) and the observation (square) against the normalised incident wave height (H_{m0}/d), while Table 4 shows the detailed number for each case. The observed:predicted comparison figure shows that both values has a good agreement for H_{m0}/d<0.45. For higher H_{m0}/d, however, the results look a little bit inconsistence with test no. 40205 and 40206 (Table 4) showing an underprediction and test no. 40207 (Table 4) showing an overprediction.

This can be explained by comparing a conventional vertical breakwater and an OWC installed vertical breakwater configuration. Unlike the conventional one, an OWC installed

263 breakwater has a front wall opening and in-chamber rear wall wave reflection. Unlike a front
264 wall reflection, the in-chamber rear wall reflection may be delayed in timing. This condition
265 then cased the reflected wave to act just like an 'imaginary' berm to the incoming wave. The
266 existence of this 'imaginary berm' may then 'pushed' the incident waves into a breaking state
267 for cases 40205 and 40206, thus explaining the un-safe prediction, and also 'pushed' the
268 breaking incident wave into its broken state in 40207 case, thus explaining the over-
269 estimation. It is worth noting that the berm is assumed to be null, in current prediction
270 process.

271 The orifice settings, furthermore, don't seem to have a consistent impact on the number of
272 impacts observed on the front wall. Test numbers 32801 and 31704 for example show an
273 increase in number of impacts observed, while case numbers 32709 and 40203 show a
274 decrease in number of impacts. This could have happened due to the 'imaginary' berm
275 explained. Different orifice settings may result in different in-chamber rear wall reflection,
276 thus may have different effect to the incoming wave. Unfortunately, current limited number
277 of orifice opening is not sufficient to look for such influence. Nevertheless, the prediction
278 methods proposed by Calabrese and Vicinanza (1999) can be used quite well for $H_{m0}/d<0.45$.

279 **In-chamber wave loads – ceiling impact characterisation**

280 Unlike the front wall, in the idealised view of the in-chamber water column, the in-chamber
281 ceiling would never experience a wave pressure directly from the incident wave except in the
282 event where the whole water column rises up and meets the ceiling. Under normal operating
283 conditions, the ceiling should only experience the air pressure generated inside the chamber.
284 This will be the case if the water column is behaving well as demonstrated in Figure 14. In-
285 chamber video observation, however, shows a *sloshing* phenomenon occurring during some
286 of the experiments. This phenomenon is characterised by a rough turbulent surface water
287 movement inside the chamber, with an impact on the chamber ceiling in some extreme cases.

Four different regimes are now proposed to differentiate the in-chamber water column movement inside the chamber. The first one is "well-behaved" water column movement as previously illustrated in Figure 14. The second is "low sloshing" where the water column vertical oscillation is still easily observed, but the water surface is not calm (Figure 15). The third level is "medium sloshing" where the water column vertical movement is harder to distinguish and there is an obvious difference in water level between the front and the rear parts of the water column, as apparent in Figure 16. The final and probably most important characterisation is the "violent movement" where there is a very little water column oscillation visible while the water surface is very chaotic. In some extreme cases, impact pressures are measured on the ceiling during this level of water column movement as shown in Figure 17.

In addition to the water column behaviour characterisation, three types of violent ceiling impact were observed. The first type is the one generating highest impact pressure of up to $12\rho g H_{m0}$, which is "single ceiling impact" on the front or the rear part of the chamber. Figure 18 (a) shows the single impact event pressure measurements inside the chamber, (b) shows the location of each corresponding colour, and (c) shows the corresponding image of impact on the rear part of the chamber ceiling. In addition to the high magnitude of impact, this condition is worsened by the unpredictability of the impact pressure generated as shown by the bigger pressure measurement in Figure 19, even though the wave condition has lower wave steepness. The impact, unfortunately, cannot be seen in the video record because the location of the impact is very close to the in-chamber video recorder location.

The second type of violent ceiling impact is "successional ceiling impact" where there is, in succession, either an impact on the rear of the ceiling followed by an impact in the front of the chamber, or *vice versa*. Figure 20 (a) to (d) show the breakdown of this type of ceiling impact with t^* indicates time within each breakdown event relative to a single wave period

313 ($t^* = t/T_p$). In the example figure, the impact occurs on the front part of the ceiling, directly
314 followed by an impact on the rear part of the ceiling. Figure 21 shows the pressure time series
315 on the ceiling and the rear wall of the chamber. The (a) to (d) red arrows show the physical
316 processes corresponding to events within the time history in Figure 20. The water column
317 movement observed between Figure 20 (c) and (d) shows a very similar flip-through motion
318 as described by Lugni *et al.* (2006). The sudden turning of the horizontal water flow into a
319 vertical jet which impacted the ceiling. The time series pressure measurement (Figure 21)
320 indicates that, although there is an impact pressure observed on the rear wall (P10 – solid
321 green line), the impact occurs on the ceiling is much greater. Lugni et al. (2006), furthermore,
322 observed a very high vertical jet acceleration of up to 1500 times the gravity acceleration,
323 using Particle Imaging Velocimetry (PIV) technique, during the experiment. This may
324 explain the higher impact pressure experienced by the ceiling due to the kinetic energy of the
325 vertical water jet.
326 Figure 22 is a second example of a "successional celling impact", but this time, with the first
327 impact occurring on the rear part of the ceiling followed by the impact on the front part. In
328 this instance, the impact pressure maxima generated are similar between the two successive
329 impacts.
330 The third ceiling impact type is the "whole water column ceiling impact" when the whole, or
331 nearly the whole water column hits the ceiling of the chamber. This type of ceiling impact is
332 usually indicated by a rising non-impulsive wave pressure before and after the impact pressure,
333 with the impact occurring at the peak of the chamber pressure. Figure 23 shows a pressure time
334 series of such an event under regular a wave condition. As can be seen, the non-impulsive
335 pressure is similar, if not identical, for each single wave cycle. The impact magnitude, however,
336 looks random. This further emphasises the uncertainty in ceiling impact. Because the method
337 for the estimation of the percentage of impacts has been shown to work quite well for the front

wall of the OWC breakwater, it is interesting to explore whether the ceiling impacts have any connection with the front wall impacts. Table 5 summarises the impact force maxima ($F_{i,max}$), time of the force maxima ($t_{i,max}$) and rise time (t_r) for both the front wall and in-chamber ceiling for seven large ceiling impact cases. One important similarity that all of the cases share is that they are closer to the fully open regime (bigger orifice diameter), although not all with the same orifice opening. This is possible because the chamber pressure generation is much less in the bigger orifice opening, so larger water column motion is anticipated. Furthermore, the force impact maxima are consistently larger on the ceiling than the front wall and are accompanied by much shorter rise times (t_r). Biggest impacts occurring on the front wall, on the other hand, do not generally result in the biggest impacts on the ceiling - all of the $t_{i,max}$ for the front and the ceiling are different, apart from case number 3. Cases number 3 and 4 share the same wave condition with the difference only in the orifice opening. The force impact maximum on the front wall is shown to occur at the same time (4727s) in both tests. The two ceiling impact maxima, however, occurred at different times (4728s and 3718s). This further emphasises the uncertainty in impact force experienced by the ceiling. From the albeit somewhat limited set of impact cases studied, the observation shows that in the fully open condition, under conditions that give impacts on the front wall, there will be impacts on the ceiling too.

Figure 24 compares, for each test, the front wall and in-chamber ceiling force maxima for non-impulsive loads and impulsive (impact) loads. Data located above the solid line means the in-chamber ceiling impact force maxima exceeds the front wall impact force maxima for the given test. As can be seen, almost all points are located above the solid line. This demonstrates that in-chamber impact forces are at least comparable with and potentially just as important as the front wall impacts.

Figure 25 shows a similar comparison, now for the rear wall and in-chamber ceiling impact force maxima comparison, while Figure 26 shows the front wall and rear wall impact force

363 maxima comparison. It is apparent that the ceiling impact force maxima are always bigger
364 than the impact force experienced by the rear wall (data located above the solid line).

365 **In-chamber wave loads – wave conditions at risk**

366 The exploration is extended to map the wave conditions at risk of chaotic water column
367 movement. For this study, the observation is extended to regular wave conditions shown in
368 Figure 27.

369 For each test, the sloshing regime was identified and recorded alongside the wave height or
370 significant wave height (H or H_{m0}), chamber width (B_c/L), and the opening:chamber ratio
371 (A_o/A_c). A colour code is utilised to indicate the sloshing intensity observed. If the water
372 surface looks calm while oscillating (Figure 14), then it is recorded as "no sloshing" and it is
373 represented in green. Blue represents "low sloshing", the condition where the water surface is
374 not calm (Figure 15), but the oscillation is still obvious within the video. Yellow indicates
375 "medium sloshing" with a very visible water height difference between the front and the rear
376 end of the chamber while the oscillating motion is still visible (Figure 16). Finally, red
377 indicates "violent movement" where the water movement inside the chamber is very violent
378 with almost no obvious water oscillation observed within the video (Figure 17). In addition to
379 the colour code, several symbols are used for additional information: no test available (/),
380 water level touches the ceiling (^), and major ceiling impact observed (!).

381 The results for the sloshing regime for the regular wave conditions can be seen in Figure 28.
382 One characteristic that can be seen right away is that, as expected sloshing is more likely to
383 occur with the bigger orifice openings. The chamber pressure generated by the smaller orifice
384 (the closed case condition included) inhibits the water column from sloshing, although some
385 low sloshing phenomena still can be observed in some of the cases. It is also clear from the
386 result that when low sloshing occurs in the closed/near-closed chamber conditions, there is

likely to be a higher sloshing in the corresponding bigger orifice condition. In general, sloshing is more likely to occur in higher wave height conditions.

In order to explore any influence of the of the front wall penetration, the curtain used as the front wall of the physical model structure was lowered for the 0.88% orifice:chamber area ratio case. The results show that it has some effect for the B_c/L = 0.1394 cases. It changes the sloshing condition from low sloshing (blue) to no sloshing (green) for the H = 0.26 m and H = 0.52M cases. The lower curtain wall also causes change from medium sloshing (yellow) to low sloshing (blue) for the H = 0.78m case. This influence, however, does not seem to appear in the smaller B_c/L cases. For example, for the B_c/L = 0.1045 and 0.8m, both the original and lowered curtain wall cases regain the same level of sloshing intensity, even though the impact pressure observed in the H = 0.8 m original curtain height did not appear in the lowered curtain case. Interestingly, the converse is observed for the B_c/L = 0.0697 and H = 0.67m case where the sloshing intensifies from the medium sloshing (yellow) to the high sloshing (red) state. Nevertheless, lowering the front wall usually has a generally calming impact to the sloshing characteristics.

Figure 29 shows the observations for the irregular wave conditions. The wave height listed in the figure is the nominal significant wave height (H_{m0}) and the wavelength (L_p) in the relative chamber width is calculated using fictitious significant wave period. The irregular wave conditions seem to exacerbate the water column condition inside the caisson – in all cases, a higher sloshing intensity is observed compared to the corresponding regular waves case. The trend, however, remains the same with the sloshing more likely to occur for higher wave heights and bigger orifice openings.

Conclusions

Established design tools for the prediction of wave loads acting on a conventional vertical breakwater were tested against the large-scale measurements of the OWC caisson front wall wave loads. The comparison was done for both non-impulsive and impulsive (breaking) wave loads. Under non-impulsive condition, a comparison between the measurements and Goda's prediction method show that introducing an OWC into a vertical breakwater resulted in a more conservative prediction with the measurement consistently being below the Goda predicted values.

The comparison was then done for impulsive wave loads. Impact force maxima and rise times were shown to follow the relationship proposed by Weggel and Maxwell (1970) with magnitude and rise time relationship similar with the relationship in a conventional vertical breakwater as shown by Cuomo *et al.* (2010a; 2011).

Bagnold number (B_a) analysis showed that an adjustment factor (λ) of 5.3 needed to be used to compensate for the scaling effect in this case. The number of front wall impacts observed during the experiment is also shows that Calabrese and Vicinanza (1999)'s method to predict the proportion of wave breaking within an irregular wave train can be used to predict the number of impacts experienced by an OWC installed vertical breakwater with a good agreement.

Next, in-chamber ceiling impacts were explored, both qualitatively and quantitatively. The observations resulted in the characterisation of three different types of impact: (a) "single ceiling impact" on the front or the rear part of the ceiling, (b) "successional ceiling impacts" either from the front follow by the rear part of the ceiling or *vice versa*, and (c) "water column ceiling impact" where the whole water column rose and hit the ceiling. The results showed that "single ceiling impact" gives the highest impact pressures with impact pressure

433 reached up to $12\rho gH$ during the large-scale measurements, followed by the "successional
434 ceiling impacts". When compared with the front wall impact force in the same event, it shows
435 that the in-chamber ceiling impact pressure is at least comparable with that on the front wall.

436 To check the behaviour of the in-chamber water column during operation, in-chamber video
437 recording was utilised. The in-chamber water column movement can be classified into four
438 intensity levels: well-behaved, low sloshing, medium sloshing, and violent movement
439 conditions, with in-chamber ceiling impacts observed during the violent movement condition.
440 The wave conditions at risk have been mapped and the observation showed that the violent
441 water column movement is more likely to occur with the bigger orifice openings and with
442 higher wave height.

443 **Acknowledgments**

444 For the original GWK tests, the authors would like to say thank to University of Edinburgh,
445 HR Wallingford, University of Campania "Luigi Vanvitelli", Queen's University Belfast, and
446 University of East Anglia for supporting staff time and to Drs. John Alderson (HR
447 Wallingford), Viviana Russo (Queen's University of Belfast), Vincenzo Ferrante (Second
448 University of Naples), Matthias Kudella (GWK) and the GWK team for design, construction,
449 and testing during the experiments. The authors also would like to say thank you to Professor
450 Trevor Whittaker (Queen's University Belfast) and Dr Mark Cooker (University of East
451 Anglia). The funding for GWK facility is provided by the European Community's Seventh
452 Framework Progamme through the Integrating Activity HYDRALAB IV, Contract no 261520.
453 Krisna Pawitan also would like to express his gratitude to Indonesia Endowment Fund for
454 Education (LPDP) for the financial support for his studies in Edinburgh.

455 **Data Availability**

All data used during the study are available from the corresponding author, Hydralab repository, or GWK manager by request: front wall and in-chamber rear wall wave pressure data; in-chamber water column condition during operation.

References

Allsop, N.W.H., McKenna, J.E., Vicinanza, D. and Wittaker, T.J.T., 1996a. New design methods for wave impact loading on vertical breakwaters and seawalls. Coastal Engineering Proceedings, 1(25). (ASCE).

Allsop, N. W. H., Vicinanza, D., and McKenna, J. E., 1996b. Wave forces and vertical and composite breakwater.HR Wallingford: Report SR 443

Ashlin, S.J., Sundar, V. and Sannasiraj, S.A., 2017. Pressures and forces on an oscillating water column–type wave energy caisson breakwater. Journal of Waterway, Port, Coastal, and Ocean Engineering, 143(5), p.04017020.

Bagnold, R.A., 1939. Interim report on wave-pressure research. *Excerpt from the J. of the Institution of Civil Engineers*.

Bullock, G.N., Obhrai, C., Peregrine, D.H. and Bredmose, H., 2007. Violent breaking wave impacts. Part 1: Results from large-scale regular wave tests on vertical and sloping walls. *Coastal Engineering*, *54*(8), pp.602-617.

Calabrese, M and Vicinanza, D., 1999. Prediction of wave impact occurrence on vertical and composite breakwater. Excerpta of Italian contributions to the field of hydraulic engineering, Vol.XIII, 25pp., ISSN 0394-526X.

Cuomo, G., Allsop, W., Bruce, T. and Pearson, J., 2010a. Breaking wave loads at vertical seawalls and breakwaters. *Coastal Engineering*, *57*(4), pp.424-439

Cuomo, G., Allsop, W. and Takahashi, S., 2010b. Scaling wave impact pressures on vertical walls. *Coastal Engineering*, *57*(6), pp.604-609.

480 Cuomo, G., Piscopia, R. and Allsop, W., 2011. Evaluation of wave impact loads on caisson
481 breakwaters based on joint probability of impact maxima and rise times. *Coastal Engineering*, *58*(1),
482 pp.9-27.

483 Faraci, C., Scandura, P. and Foti, E., 2014. Reflection of sea waves by combined caissons. *J.*
484 *Waterway, Port, Coastal, and Ocean Engineering*, *141*(2), p.04014036.

485 Goda, Y., 1974. New wave pressure formulae for composite breakwaters. Coastal Engineering
486 Proceedings, 1(14). (ASCE).

487 Goda, Y., 2010. *Random seas and design of maritime structures*. World Scientific Publishing
488 Company.

489 Hattori, M., Arami, A. and Yui, T., 1994. Wave impact pressure on vertical walls under breaking waves
490 of various types. *Coastal Engineering*, *22*(1-2), pp.79-114.

491 He, F. and Huang, Z., 2016. Using an oscillating water column structure to reduce wave reflection
492 from a vertical wall. Journal of Waterway, Port, Coastal, and Ocean Engineering, 142(2), p.04015021.

493 Hiroi, I., 1919. On a method of estimating the force of waves. *Memoirs of Engineering Facility,*
494 *Imperial University of Tokyo*, *10*(1).

495 Hovarth, E., 2009 Wave loading at coastal wave energy converters. MSc Dissertation. School of
496 Engineering, University of Edinburgh

497 Hughes, S.A., 2014. Coastal engineering challenges in a changing world. Journal of Applied Water
498 Engineering and Research, 2(2), pp.72-80.

499 Hughes, S.A., 1993. Physical models and laboratory techniques in coastal engineering (Vol. 7). World
500 Scientific.

501 Jarlan, G.E., 1961. A perforated vertical wall breakwater. *The Dock and Harbour Authority*, 486,
502 pp.394-398.

503 Kirkgöz, M.S., 1995. Breaking wave impact on vertical and sloping coastal structures. *Ocean*
504 *Engineering*, *22*(1), pp.35-48.

505 Kisacik, D., Troch, P. and van Bogaert, P., 2012. Experimental study of violent wave impact on a
506 vertical structure with an overhanging horizontal cantilever slab. *Ocean Engineering*, *49*, pp.1-15.

507 Laju, K., Sundar, V. and Sundaravadivelu, R., 2005. Studies on pile supported skirt breakwater. *Proc.*
508 *Int. Conf. on Coastal Zone Management and Engineering in the Middle East, Dubai.*

509 Ling, H.I., Cheng, A.H.D., Mohri, Y. and Kawabata, T., 1999. Permanent displacement of composite
510 breakwaters subject to wave impact. Journal of waterway, port, coastal, and ocean engineering,
511 125(1), pp.1-8.

512 Lugni, C., Brocchini, M. and Faltinsen, O.M., 2006. Wave impact loads: The role of the flip-through.
513 Physics of fluids, 18(12), p.122101.

514 Lugni, C., Miozzi, M., Brocchini, M. and Faltinsen, O.M., 2010a. Evolution of the air cavity during a
515 depressurized wave impact. I. The kinematic flow field. Physics of fluids, 22(5), p.056101.

516 Lugni, C., Brocchini, M. and Faltinsen, O.M., 2010b. Evolution of the air cavity during a depressurized
517 wave impact. II. The dynamic field. Physics of Fluids, 22(5), p.056102.

518 McKenna, J. and Allsop, W., 1998. Statistical distribution of horizontal wave forces on vertical
519 breakwaters. Coastal Engineering Proceedings, 1(26). (ASCE)

520 Medina-Lopez, E., Allsop, N.W.H., Dimakopoulos, A. and Bruce, T., 2015. Conjectures on the Failure
521 of the OWC Breakwater at Mutriku. *Proc. Coastal Structures Conference, Boston, Massachusetts*.
522 (ASCE)

523 Mitsuyasu, H., 1966. Shock pressure of breaking wave. Coastal Engineering Proceedings, 1(10),
524 p.17. (ASCE)

525 Müller, G. and Whittaker, T.J.T., 1995. Visualisation of flow conditions inside a shoreline wave power-
526 station. *Ocean Engineering*, *22*(6), pp.629-641.

527 Müller, G.U. and Whittaker, T.J.T., 1993. An investigation of breaking wave pressures on inclined
528 walls. *Ocean Engineering*, *20*(4), pp.349-358.

529 Oumeraci, H., 1994. Review and analysis of vertical breakwater failures—lessons learned. *Coastal*
530 *Engineering*, *22*(1-2), pp.3-29.

Oumeraci, H., Klammer, P. and Partenscky, H.W., 1993. Classification of breaking wave loads on vertical structures. Journal of waterway, port, coastal, and ocean engineering, 119(4), pp.381-397.

Oumeraci, H., Kortenhaus, A., Allsop, W., de Groot, M., Crouch, R., Vrijling, H. and Voortman, H., 2001. *Probabilistic design tools for vertical breakwaters*. CRC Press.

Patterson, C., Dunsire, R. and Hillier, S., 2010. Development of wave energy breakwater at Siadar, Isle of Lewis. *Proceedings of the 9th international conference. Edinburgh.* pp.1-738. (Thomas Telford)

Pawitan, K.A., Dimakopoulos, A.S., Vicinanza, D., Allsop, W. and Bruce, T., 2019. A loading model for an OWC caisson based upon large-scale measurements. *Coastal Engineering*, *145*, pp.1-20.

Sainflou, G. 1928. Essai sur les digues maritimes verticals. Annales des Ponts et Caausse'es. Paris 98, 11, pp: 5-48 (in French)

Streicher, M., Kortenhaus, A., Gruwez, V., Hofland, B., Chen, X., Hughes, S. and Hirt, M., 2018. Prediction of dynamic and quasi-static impacts on vertical sea walls caused by an overtopped bore. In ICCE2018 (pp. 1-15).

Streicher, M., Kortenhaus, A., Altomare, C., Gruwez, V., Hofland, B., Chen, X., Marinov, K., Scheres, B., Schüttrumpf, H., Hirt, M. and Cappietti, L., 2017. WALOWA (wave loads on walls): large-scale experiments in the delta flume. In SCACR2017 (pp. 69-80).

Streicher, M., Kortenhaus, A., Marinov, K., Hirt, M., Hughes, S., Hofland, B., Scheres, B. and Schüttrumpf, H., 2019. Classification of bore patterns induced by storm waves overtopping a dike crest and their impact types on dike mounted vertical walls–a large-scale model study. Coastal Engineering Journal, pp.1-19.

Takahashi, S., 1988. Hydrodynamic characteristics of wave-power-extracting caisson breakwater. Coastal Engineering Proceedings, 1(21). (pp. 2489-2503).

Takahashi, S., Tanimoto, K. and Miyanaga, S., 1985. Uplift wave forces due to compression of enclosed air layer and their similitude law. *Coastal Engineering in Japan*, *28*(1), pp.191-206.

Topliss, M.E., Cooker, M.J. and Peregrine, D.H., 1993. Pressure oscillations during wave impact on vertical walls. In Coastal Engineering 1992 (pp. 1639-1650).

557 Vicinanza, D., Di Lauro, E., Contestabile, P., Gisonni, C., Lara, J. L., Losada, I. J. 2019. Review of
558 Innovative Harbor Breakwaters for Wave-Energy Conversion, Journal of Waterway, Port, Coastal, and
559 Ocean Engineering, ISSN (print) 0733-950X (online) 1943-5460, Volume 145, Issue 4, pp. 1–18.

560 Viviano, A., Musumeci, R.E., Vicinanza, D., Foti E. 2019. Pressures induced by regular waves on a
561 large scale OWC, Coastal Engineering, ISSN 0378-3839, vol. 152, pp. 1–14 (103528).

562 Viviano, A., Naty, S., Foti, E., Bruce, T., Allsop, W. and Vicinanza, D., 2016. Large-scale experiments
563 on the behaviour of a generalised Oscillating Water Column under random waves. *Renewable*
564 *Energy*, *99*, pp.875-887.

565 Weggel, J.R., Maxwell, W.H.C., 1970. Experimental study of wave impact pressures. *Proc. the*
566 *Second Annual Offshore Technology Conf., OTC 1244*, Houston.

567

568

569 *Figure 1 Damage on the OWC installed breakwater at Mutriku caused by storm, showing (a) exposed chamber with the*
570 *front wall missing, and (b) some of the layer of the front wall missing greatly reducing the front wall integrity (Horvath,*
571 *2009) with permission.*

572 *Figure 2 Detailed cross section of the approximately 1:9 scale to the original OWC device. P1 to P12 indicate the location*
573 *of the pressure transducers used during the experiments. All the dimensions are in mm.*

574 *Figure 3 Photo of a wave impact event from the large-scale testing (with permission).*

575 *Figure 4 Irregular wave conditions used for the experiments at various wave steepness (diamond markers).*

576 *Figure 5 The rectangular integrated pressure (force) calculation scheme with the X_1 to X_5 locations relative to the still water*
577 *level (swl).*

578 *Figure 6 Comparison of measured ($P_{1/250}$) and predicted design pressures on the front wall, non-impulsive conditions only.*
579 *Closed chamber (circle), Ao/Ac = 0.1% (square), 0.2% (diamond), 0.88% (triangle), and 2.0% (star); and the Goda*
580 *prediction method (solid line). Wave conditions: (a) Irr01, (b) Irr02, and (c) Irr13. The zero value in y-axis indicates the*
581 *location of still water level.*

582 *Figure 7 An example of severe pressure impact characteristics with rise time (t_r) < 0.01 Tp from the large-scale model*
583 *experimental measurement with H_{m0} = 1.00m and T_p = 6s, measured at P2.*

584 *Figure 8 An example of less severe pressure impact characteristics with rise time (t_r) < 0.1 Tp from the large-scale model*
585 *experimental measurement with H_{m0} = 1.00m and T_p = 6s, measured at P2.*

586 *Figure 9 An example of near breaking pressure impact characteristics with rise time (t_r) ≈ 0.2 Tp from the large-scale model*
587 *experimental measurement with H_{m0} = 1.00m and T_p = 6s, measured at P2.*

588 *Figure 10 The definitions of rise time (t_r), duration time (t_d), and peak pressure ($p_{i,max}$) of the impact example in Figure 7.*

589 *Figure 11 Impact force maxima against rise time for the front wall impact force with the solid line represents the Weggel*
590 *and Maxwell (1970) relationship for multiple non-exceedance level after Cuomo et al. (2011).*

591 *Figure 12 Impulsive load time series measured on the front wall of the Large-scale OWC model with H_{m0} = 1.00m and T_p =*
592 *6s. Please refer to Figure 2 for P1-P5 locations.*

593 *Figure 13 Estimated (circle) and observed (square) number of impacts plotted against the normalised incident wave height*
594 *(H_{m0}), large-scale measurements, irregular waves.*

Figure 14 "Well behaved" upward (a) and downward (b) water column oscillation behaviour in T=4.0s, H=0.4m and A_o/A_c=0.1% test (with permission).

Figure 15 "Low sloshing" during upward (a) and downward (b) water column oscillation in in T=4.0s and H=0.8m and A_o/A_c=0.1% test. Regular waves (with permission).

Figure 16 "Medium sloshing" water column behaviour with less obvious upward (a) and downward (b) oscillation and an impact observed on the rear wall in (c) in T=5.0s and H=0.67m and A_o/A_c=0.88% test (with permission).

Figure 17 "Violent movement" water column behaviour with no observable water column oscillation and an impact on the ceiling in T_p=5.0 s and H_{m0} = 0.8m and A_o/A_c=2.0%. Irregular waves (with permission).

Figure 18 Example of "single ceiling impact" type with (a) Time series of chamber pressure measured with the line key in Figure 2, and (b) showing the corresponding impact event in T_p=4.0s, H_{m0}=0.4m and A_o/A_c=2.0% (with permission).

Figure 19 Example of "single ceiling impact" type with (a) time series of chamber pressure measured with the line key in Figure 2 in T_p=6.0s, H_{m0}=1.0m and A_o/A_c=0.88%. In-chamber video not available due to proximity of impact to camera resulting in obscured view.

Figure 20 (a)-(d) Sequence of events in a "successional ceiling impact (front then rear)" example in T_p=5.0s, H_{m0}=0.81m and A_o/A_c=0.88%, (a) The water column rises and is deflected by the rear wall. (b) The deflected water flows to the front part of the chamber and an impact occurs on the front part of the ceiling, followed by (c) the water column falling and (d) rising up again to give a second impact on the rear part of the ceiling. Here t indicates the relative time of each breakdown event to a single wave period ($t^* = t/T_p$) (with permission).*

Figure 21 The pressure time series of the in-chamber pressure transducers for "successional ceiling impacts" type, corresponds to the one shown in Figure 20, P6-P12 corresponds the diagram in Figure 2.

Figure 22 Pressure time series measurement example of the "successional ceiling impacts" with P6-P12 corresponds the diagram in Figure 2 in T_p=5.0s, H_{m0}=0.54m and A_o/A_c=2.0%.

Figure 23 A time series pressure measurement example of "whole water column ceiling impact", P6-P12indicates the PTs locations as shown in Figure 2 in T=6.0s, H=0.67m and A_o/A_c=2.0%. Regular waves.

Figure 24 Front wall and in-chamber ceiling force maxima comparison, for both non-impulsive (solid circles) and impulsive loads (red crosses).

Figure 25 Rear wall and in-chamber ceiling force maxima comparison, for both non-impulsive (solid circles) and impulsive loads (red crosses).

Non-exceedance level [%]	a	b	Err rel [%]
99.9	0.479	-0.411	25
99.8	0.392	-0.415	25
99.6	0.324	-0.417	25
99.5	0.307	-0.417	25
99.0	0.262	-0.414	25
98.0	0.231	-0.405	24
95.0	0.208	-0.386	24

Name	GWK	
	T_p [s]	H_{m0} [m]
Irr01	3.0	0.26
Irr02	3.0	0.39
Irr03	3.0	0.52
Irr04	4.0	0.40
Irr05	4.0	0.60
Irr06	4.0	0.80
Irr07	5.0	0.54
Irr08	5.0	0.81
Irr10	6.0	0.67
Irr11	6.0	1.00
Irr13	4.5	0.26

No	Test ref.	Wave Condition	T_p [s]	H_{m0} [m]	A_o / A_c [%]	C_r
1	32708	Irr01	3	0.26	0	0.89
2	31814		3	0.26	0.1	0.82
3	32007		3	0.26	0.2	0.66
4	32107		3	0.26	0.88	0.64
5	31410		3	0.26	2.0	0.73
6	40202	Irr02	3	0.39	0.88	0.59
7	32709	Irr03	3	0.52	0	0.9
8	40203		3	0.52	0.88	0.57
9	31902	Irr04	4	0.40	0.1	0.9
10	32008		4	0.40	0.2	0.67
11	32108		4	0.40	0.88	0.48
12	31701		4	0.40	2.0	0.52
13	32710	Irr05	4	0.60	0	0.89
14	40204		4	0.60	0.88	0.49
15	40205	Irr06	4	0.80	0.88	0.48
16	32711	Irr07	5	0.54	0	0.91
17	32009		5	0.54	0.2	0.71
18	32109		5	0.54	0.88	0.48
19	31702		5	0.54	2.0	0.52
20	40206	Irr08	5	0.81	0.88	0.5
21	32801	Irr10	6	0.67	0	0.91
22	31704		6	0.67	2.0	0.54
23	40207	Irr11	6	1.00	0.88	0.514
24	32712	Irr13	4.5	0.26	0	0.9
25	32401		4.5	0.26	0.88	0.41
26	32402	Irr14	6.5	0.40	0.88	0.48

No	Test ref.	Wave Condition	T_p [s]	H_{m0} [m]	A_o / A_c [%]	Predicted no. of impacts	no. of impacts observed
1	32708	Irr01	3	0.26	0	0	0
2	31814		3	0.26	0.1	0	0
3	32007		3	0.26	0.2	0	0
4	32107		3	0.26	0.88	0	0
5	31410		3	0.26	2.0	0	0
6	40202	Irr02	3	0.39	0.88	0	7
7	32709	Irr03	3	0.52	0	7	7
8	40203		3	0.52	0.88	4	2
9	31902	Irr04	4	0.40	0.1	0	1
10	32008		4	0.40	0.2	0	1
11	32108		4	0.40	0.88	0	1
12	31701		4	0.40	2.0	0	1
13	32710	Irr05	4	0.60	0	9	7
14	40204		4	0.60	0.88	4	12
15	40205	Irr06	4	0.80	0.88	30	40
16	32711	Irr07	5	0.54	0	2	0
17	32009		5	0.54	0.2	1	1
18	32109		5	0.54	0.88	1	2
19	31702		5	0.54	2.0	1	2
20	40206	Irr08	5	0.81	0.88	26	39
21	32801	Irr10	6	0.67	0	12	0

22	31704		6	0.67	2.0	7	5
23	40207	Irr11	6	1.00	0.88	54	28
24	32712	Irr13	4.5	0.26	0	0	0
25	32401		4.5	0.26	0.88	0	0
26	32402	Irr14	6.5	0.40	0.88	0	0

No	T_p [s]	H_{m0} [m]	A_o / A_c [%]	front			ceiling		
				$F_{i,max}$	$t_{i,max}$	t_r	$F_{i,max}$	$t_{i,max}$	t_r
1	4	0.4	2.0	5	1436.82	0.101	60	351.82	0.002
2	4	0.8	0.88	27	1328.31	0.107	51	2594.45	0.001
3	5	0.54	0.88	10	4727.53	0.384	41	4728.24	0.001
4	5	0.54	2.0	10	4727.01	0.353	61	3718.74	0.001
5	5	0.81	0.88	50	3178.47	0.082	78	4595.52	0.001
6	6	0.67	2.0	12	3954.09	0.454	84	282.59	0.001
7	6	1	0.88	76	999.44	0.025	120	1277.01	0.001

Figure 2

Click here to access/download;Figure;Figure 2.pdf

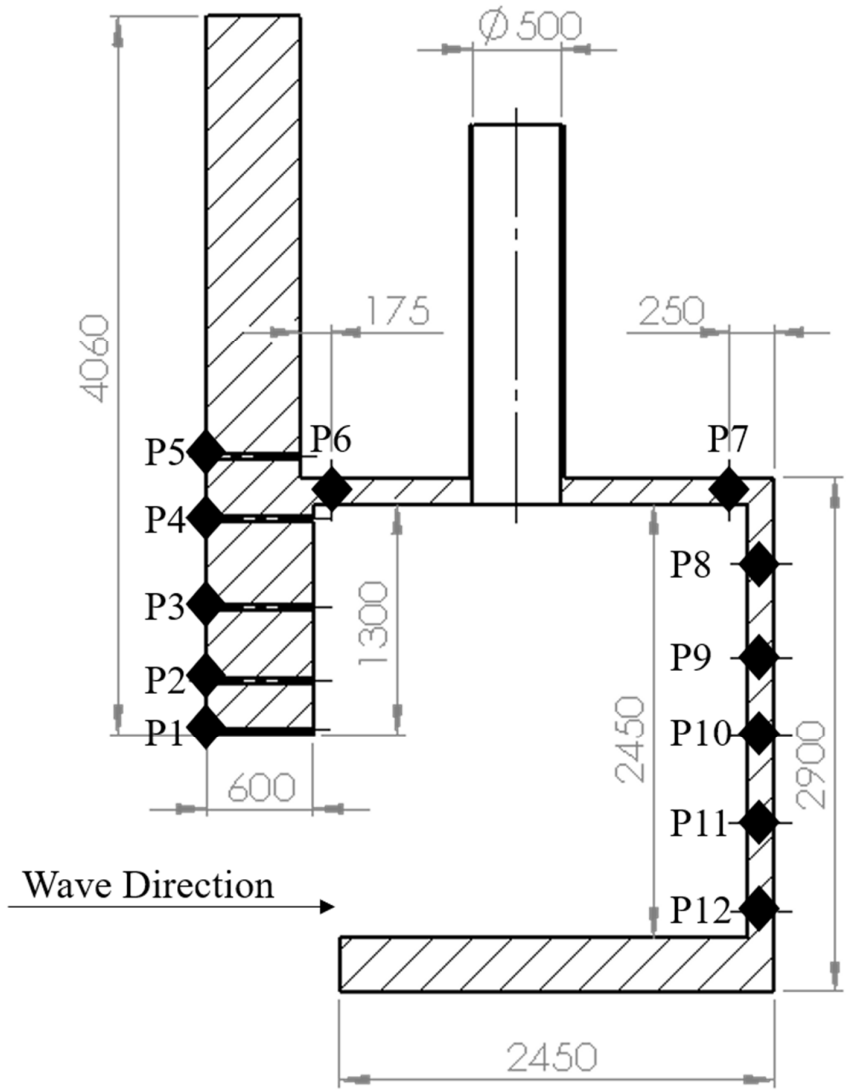

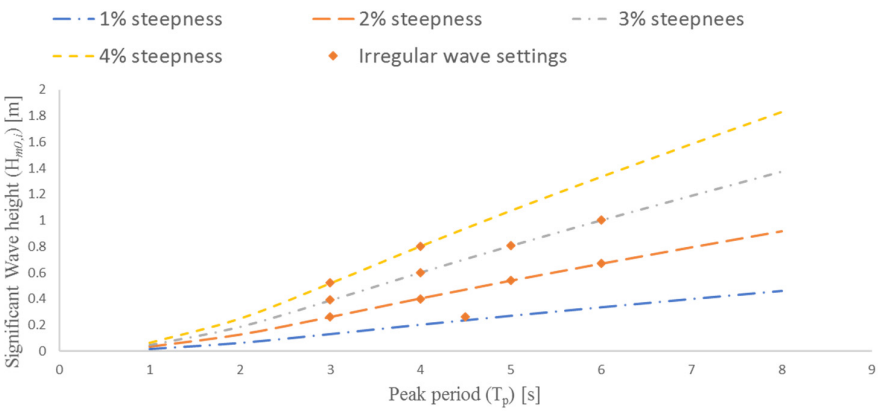

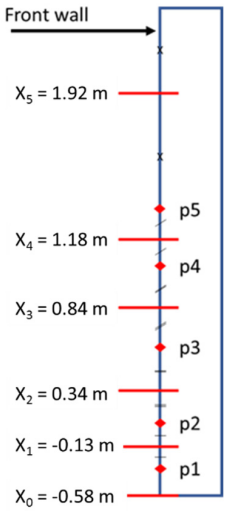

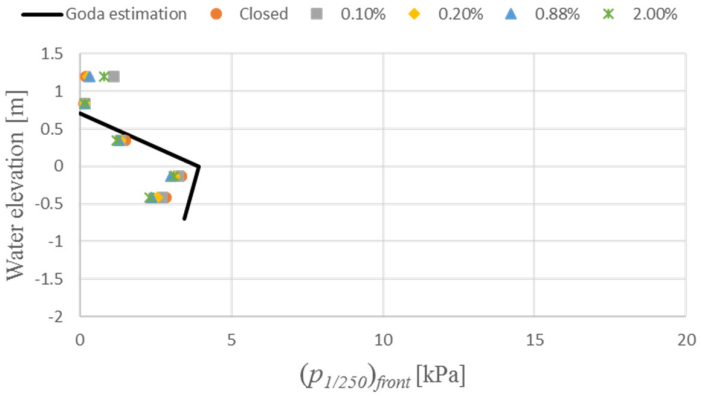

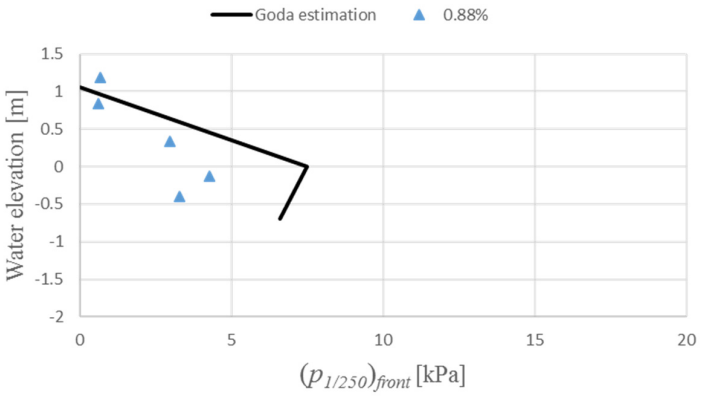

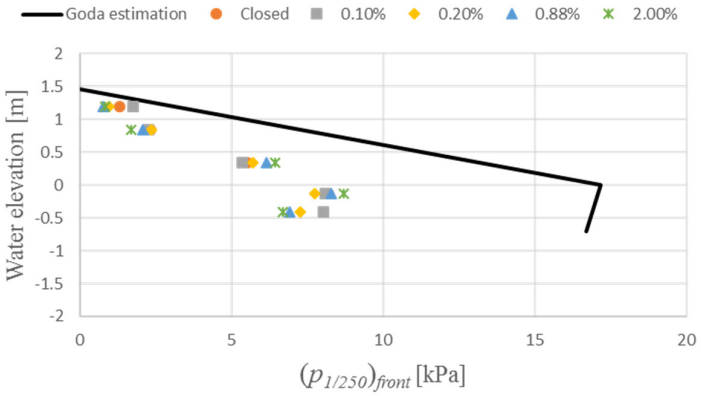

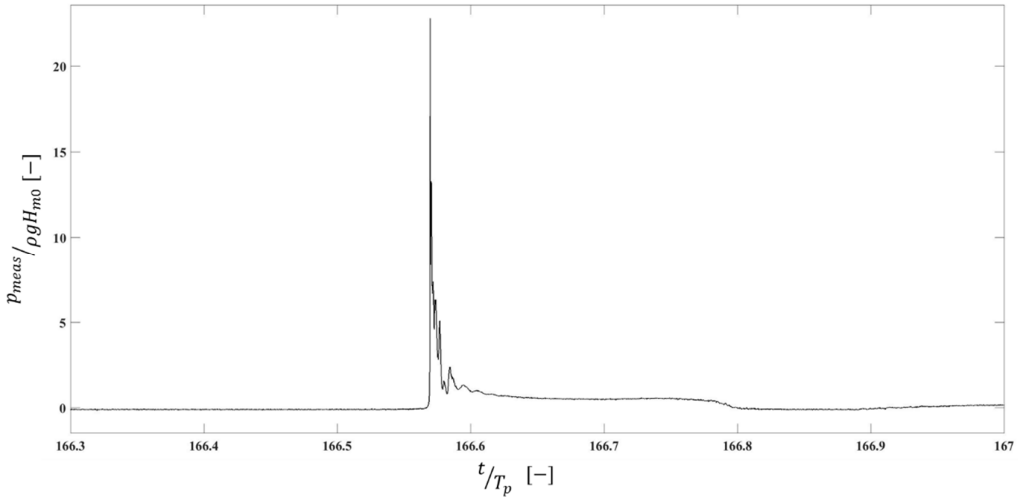

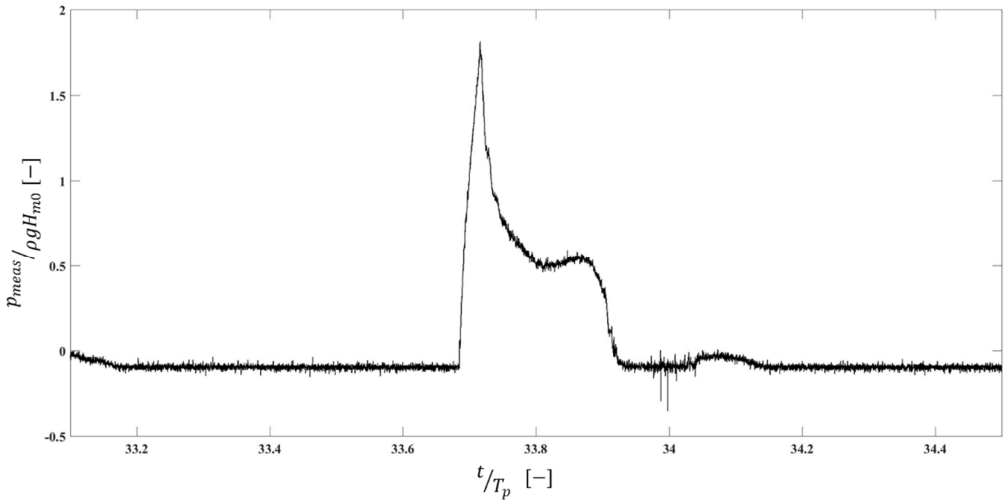

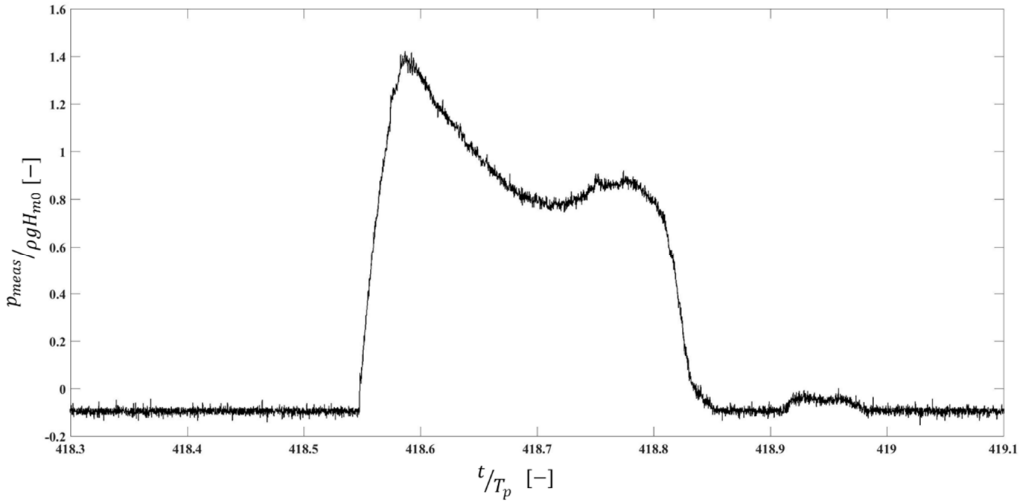

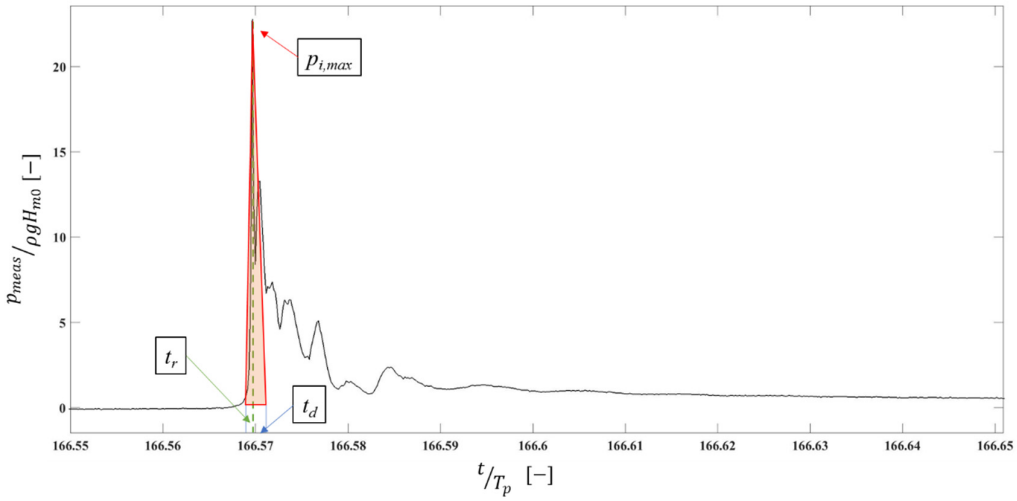

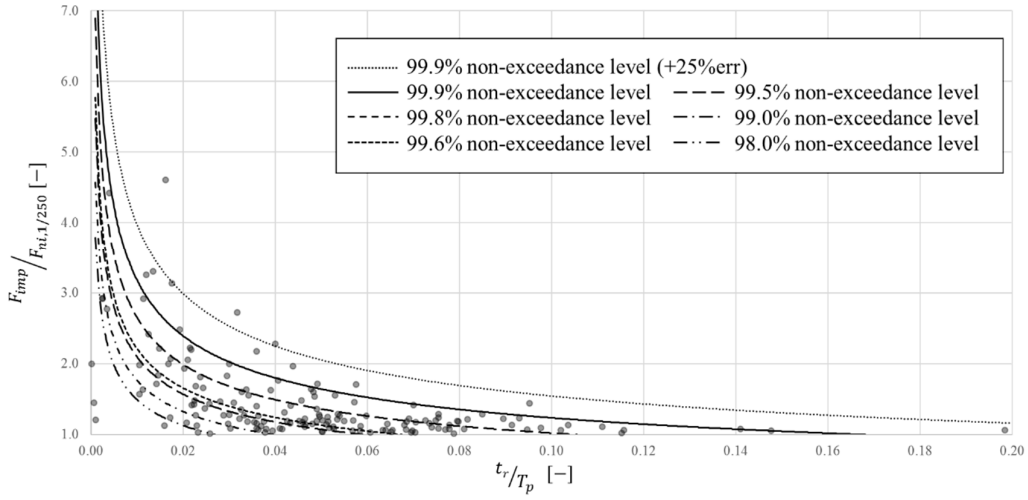

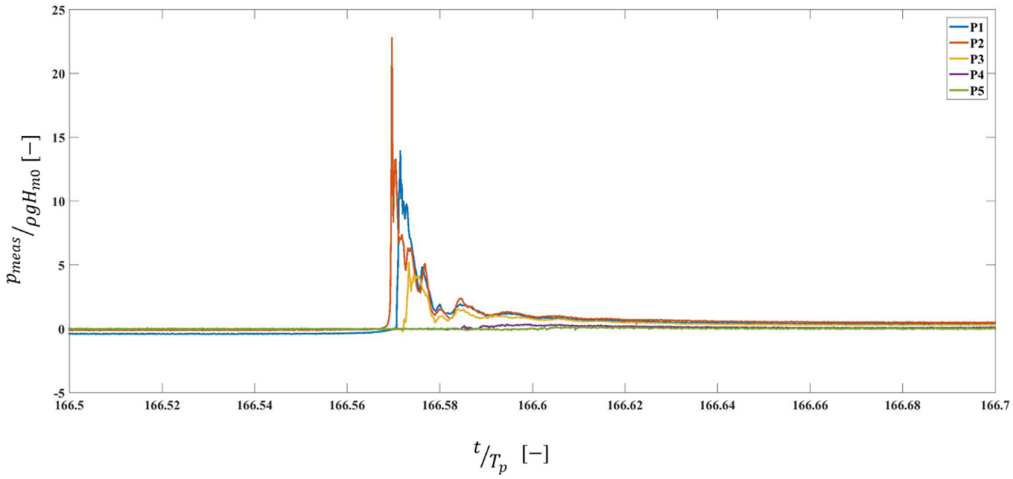

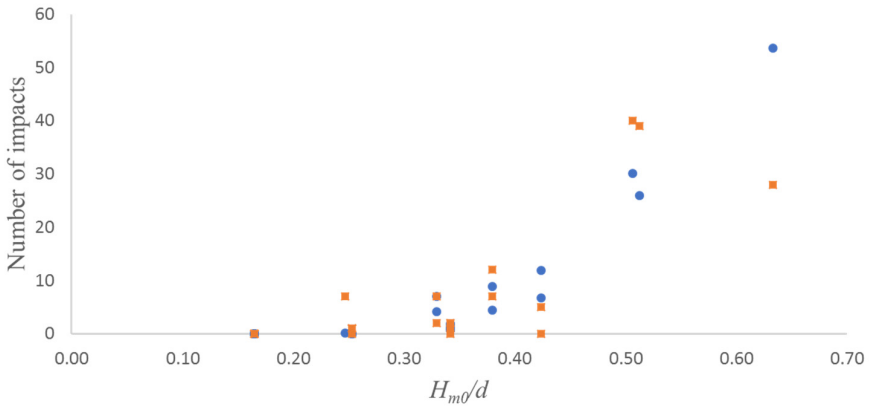

Click here to access/download;Figure;Figure 14a.pdf

Click here to access/download;Figure;Figure 15a.pdf

Click here to access/download;Figure;Figure 15b.pdf

Click here to access/download;Figure;Figure 17.pdf

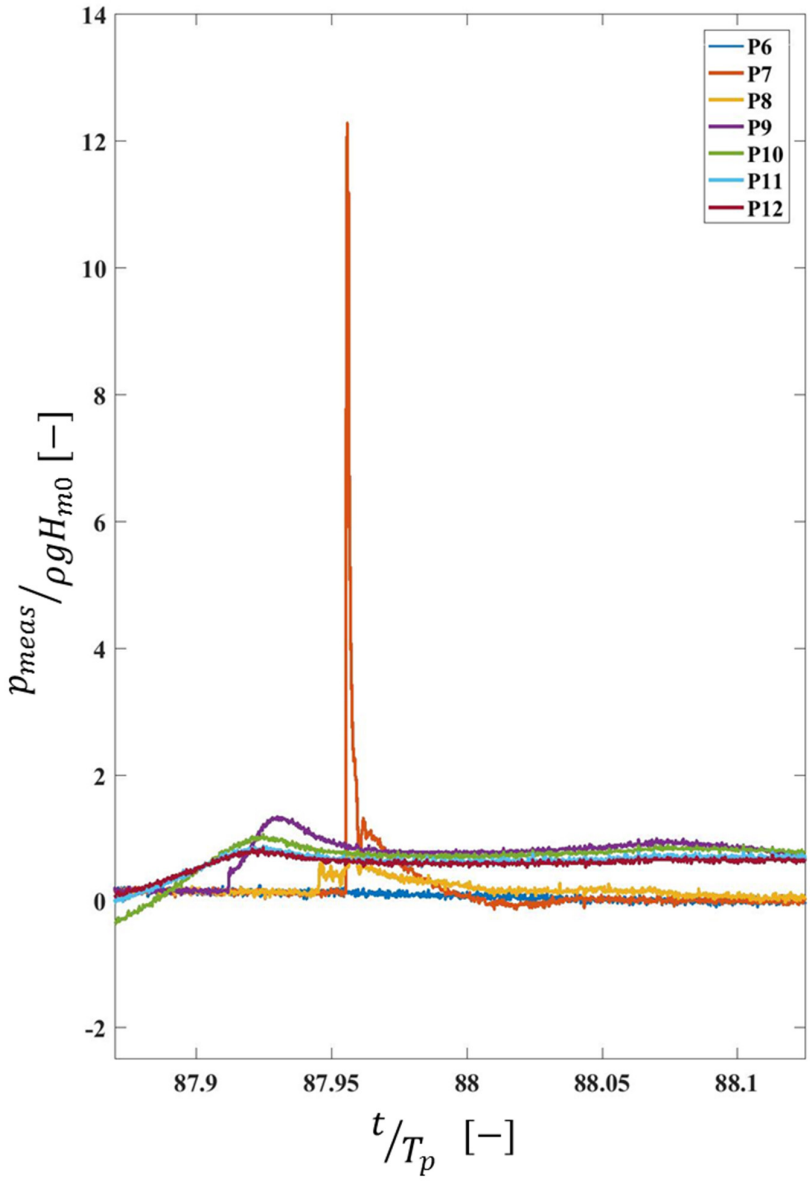

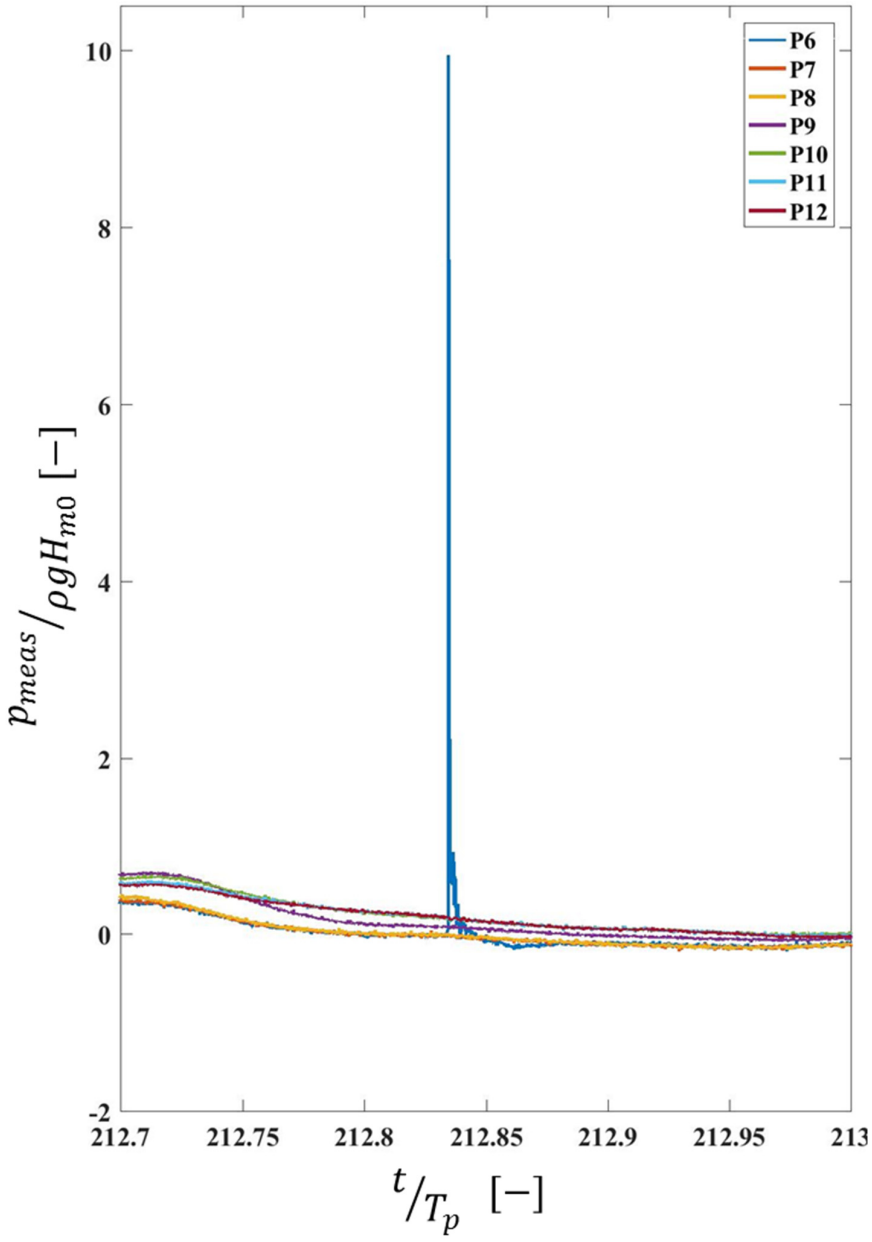

Click here to access/download;Figure;Figure 20a.pdf

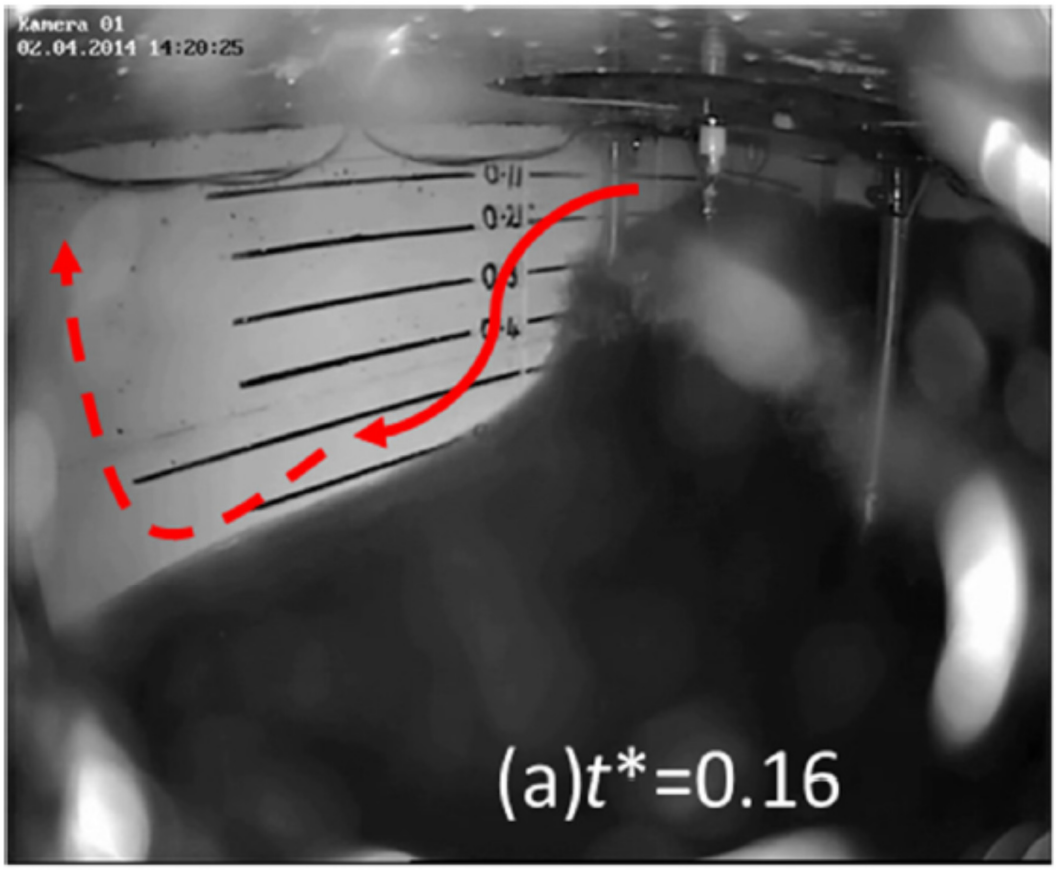

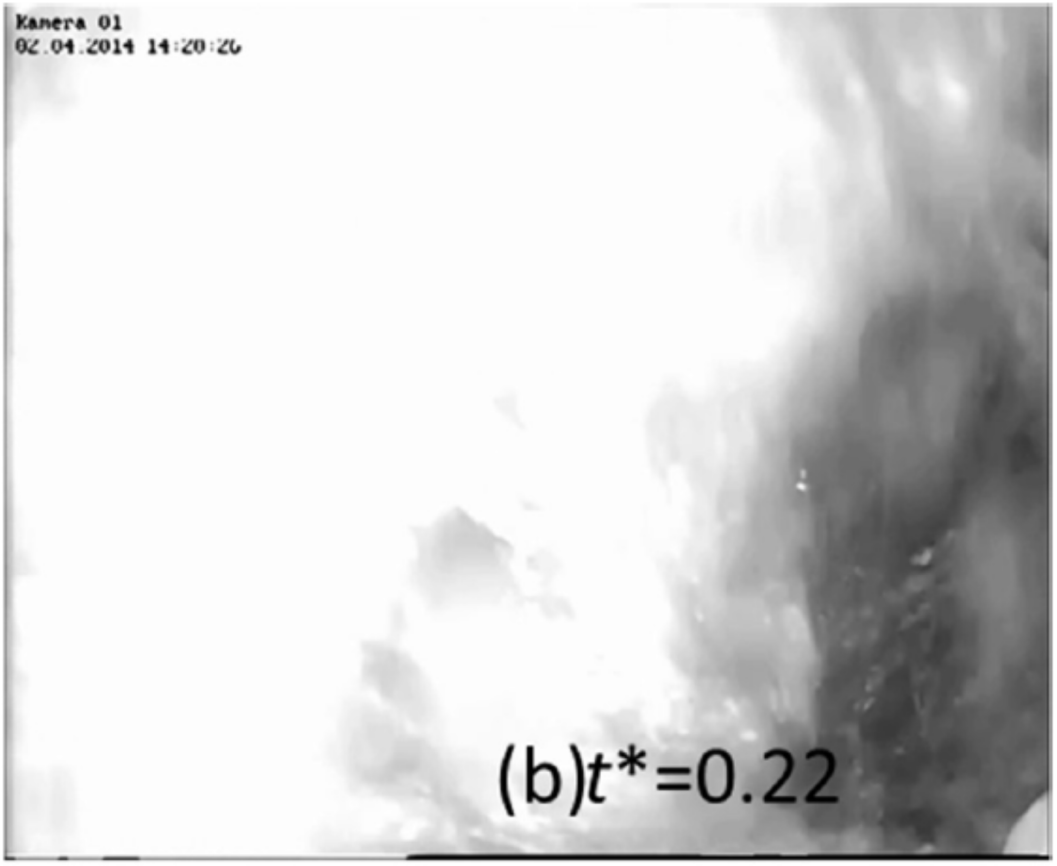

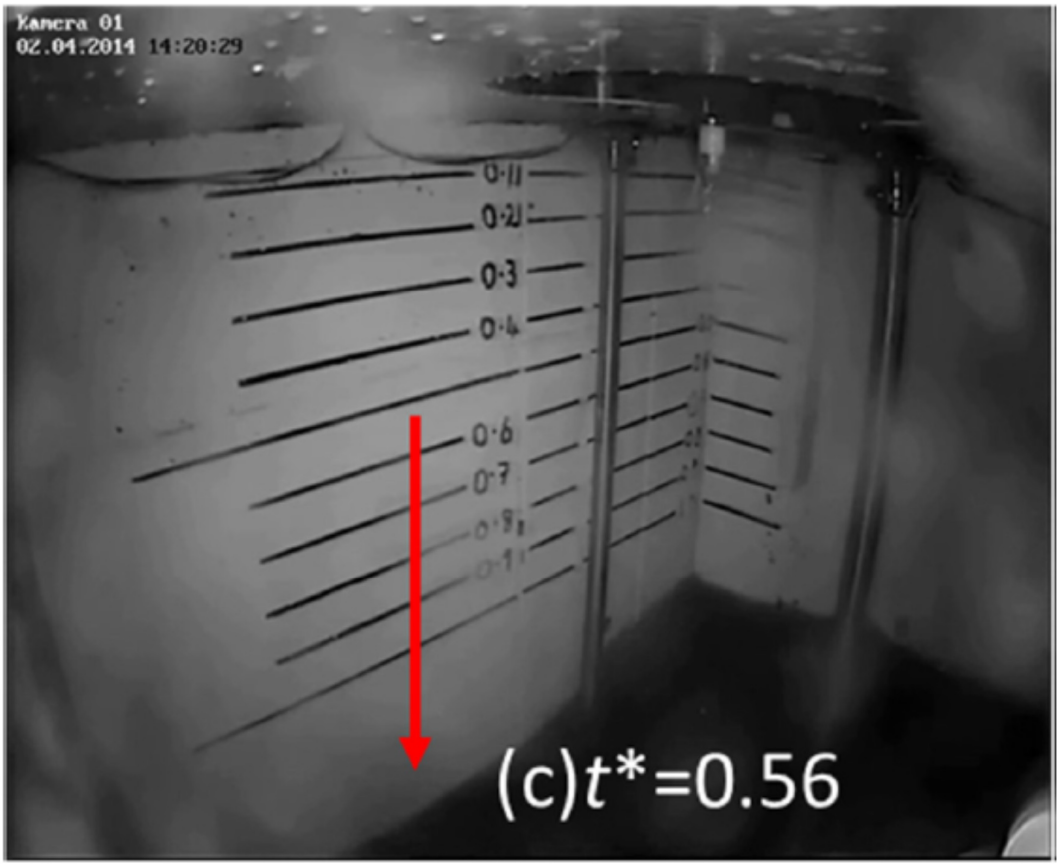

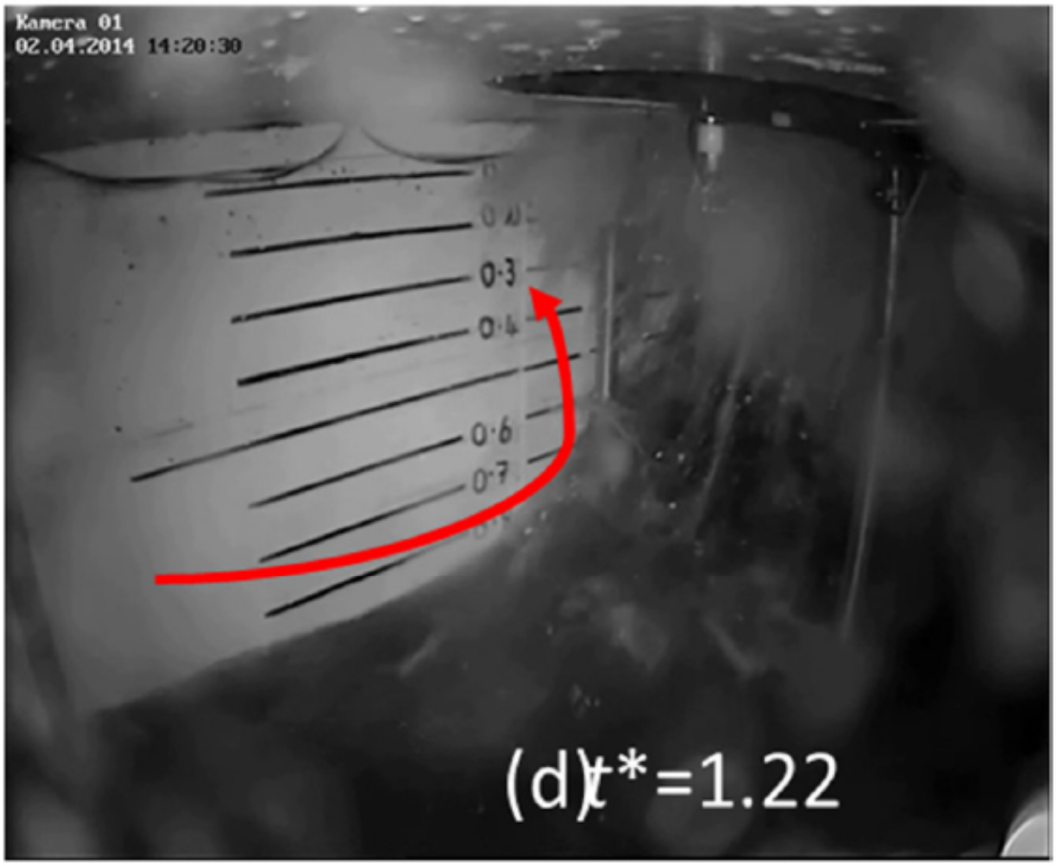

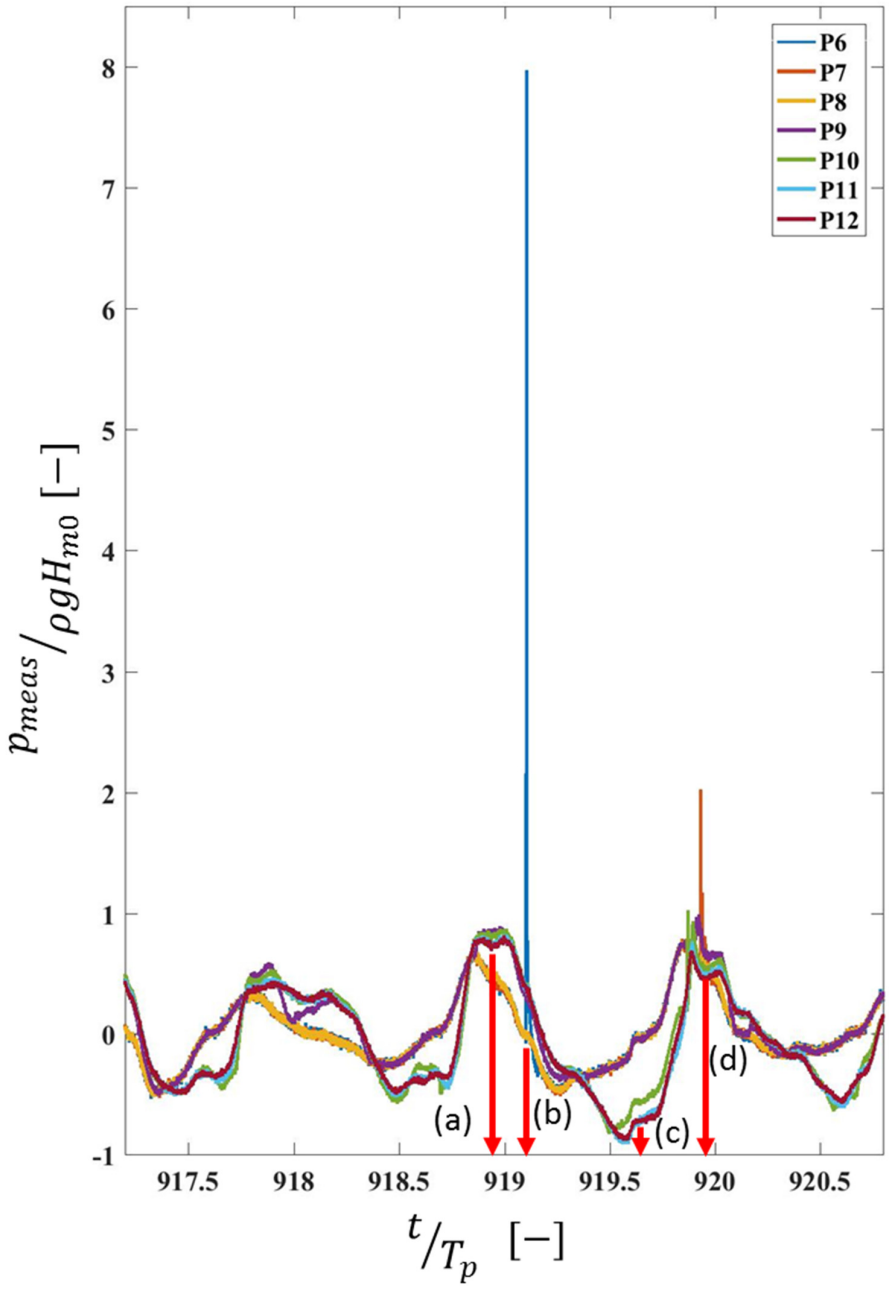

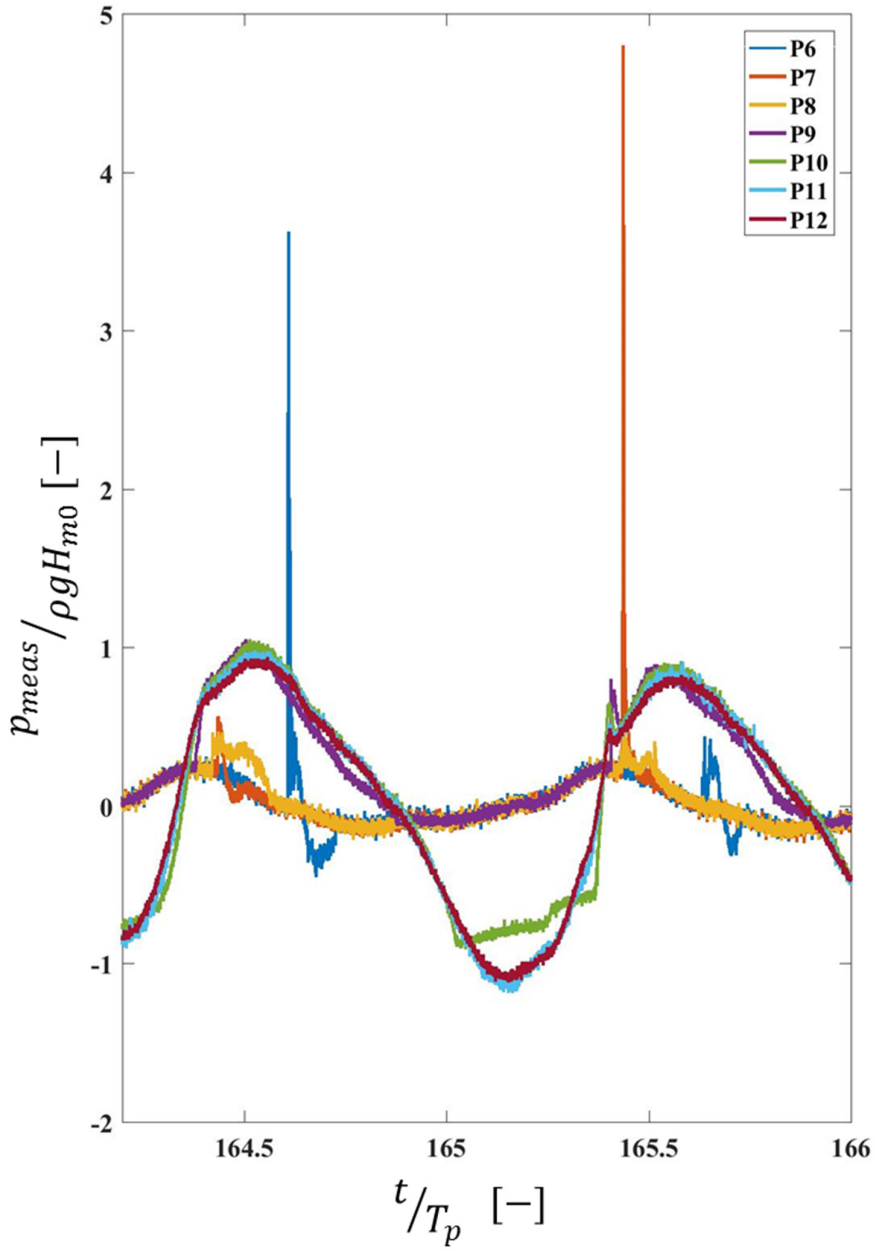

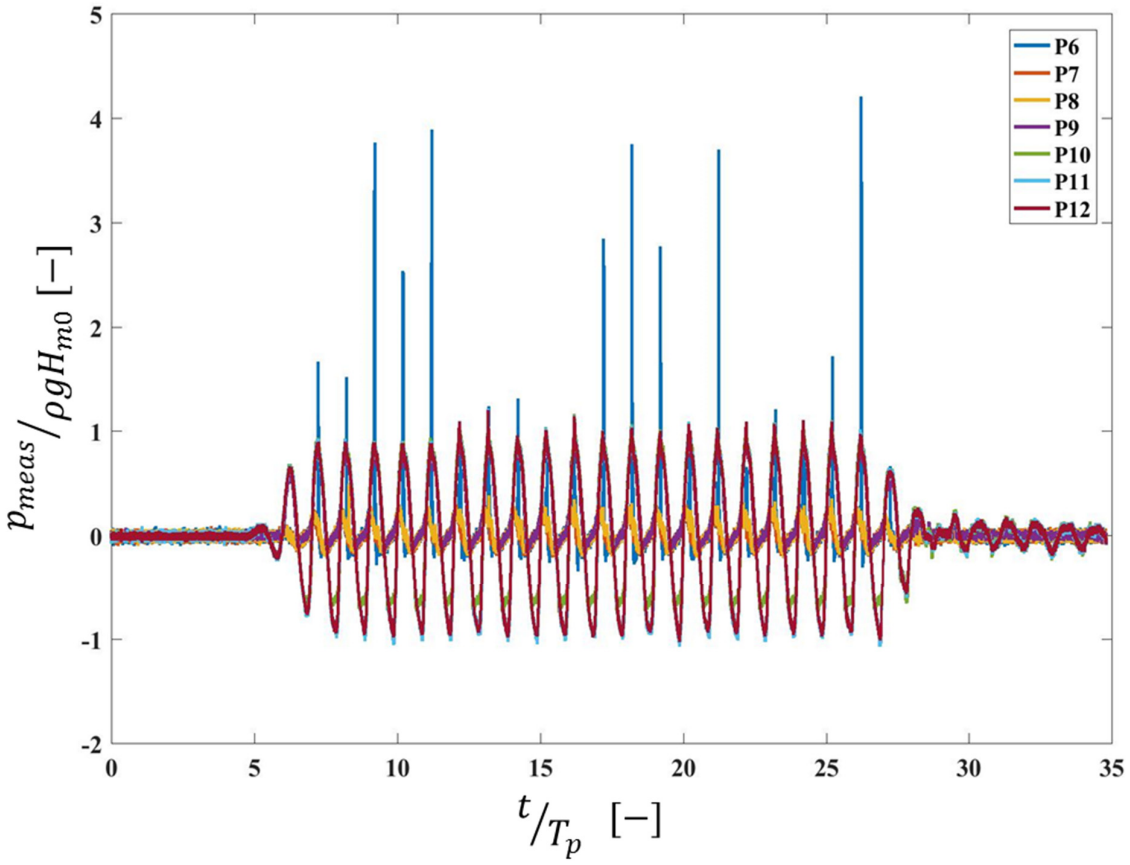

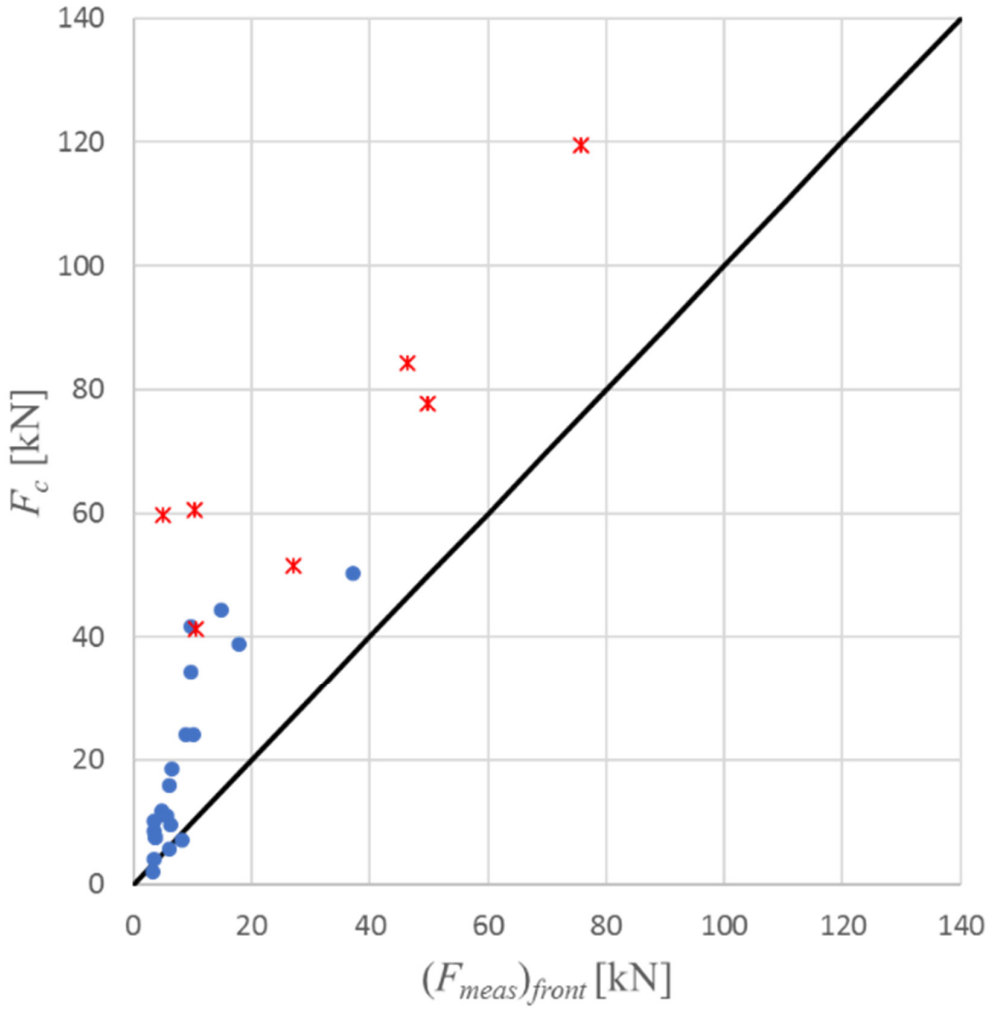

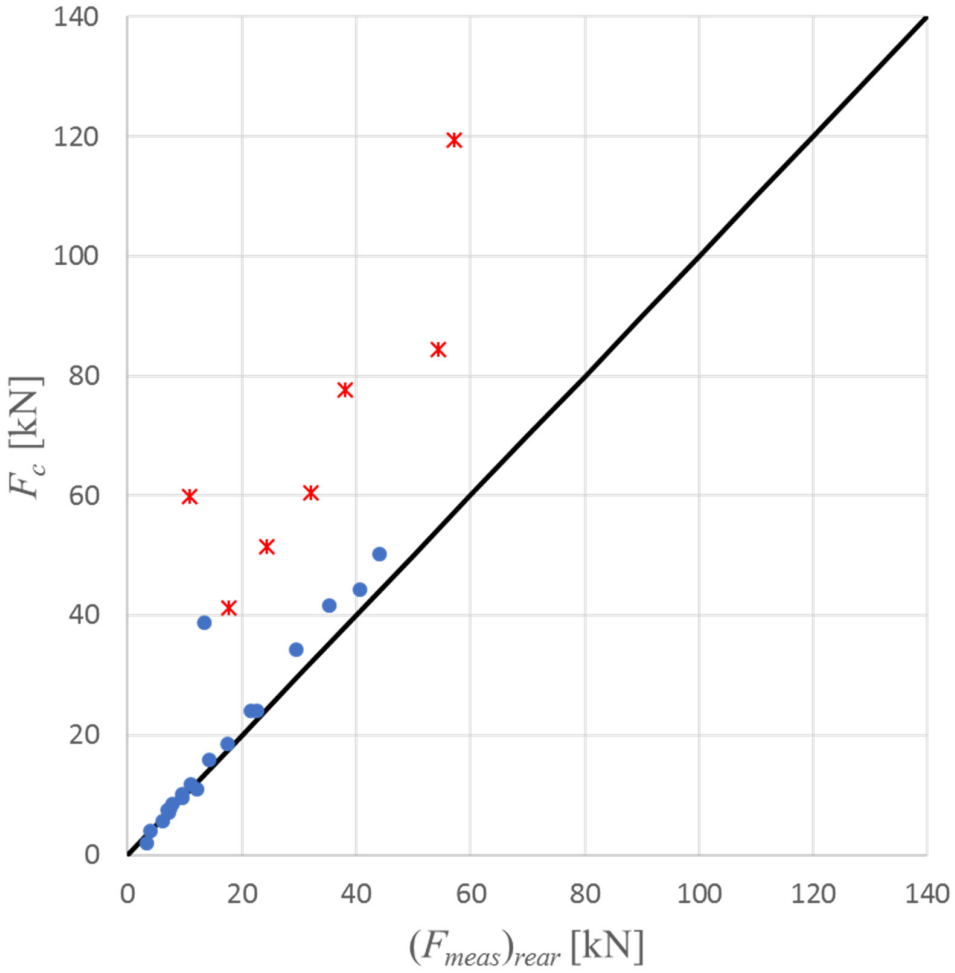

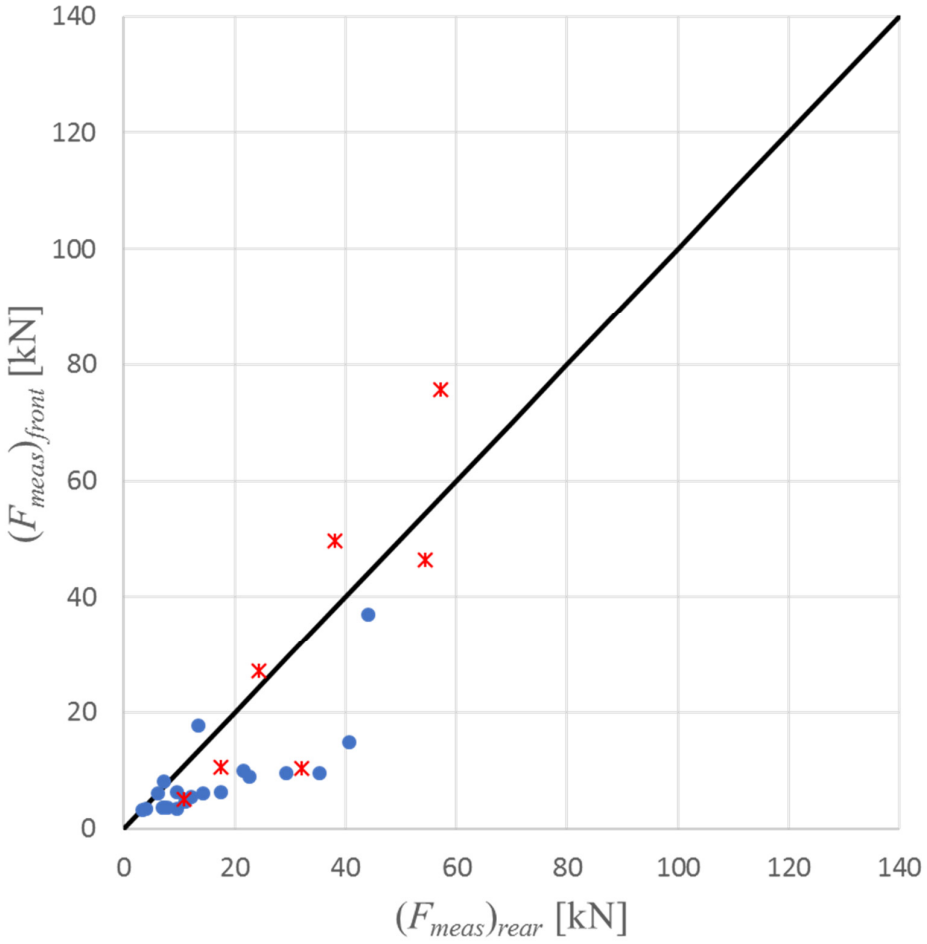

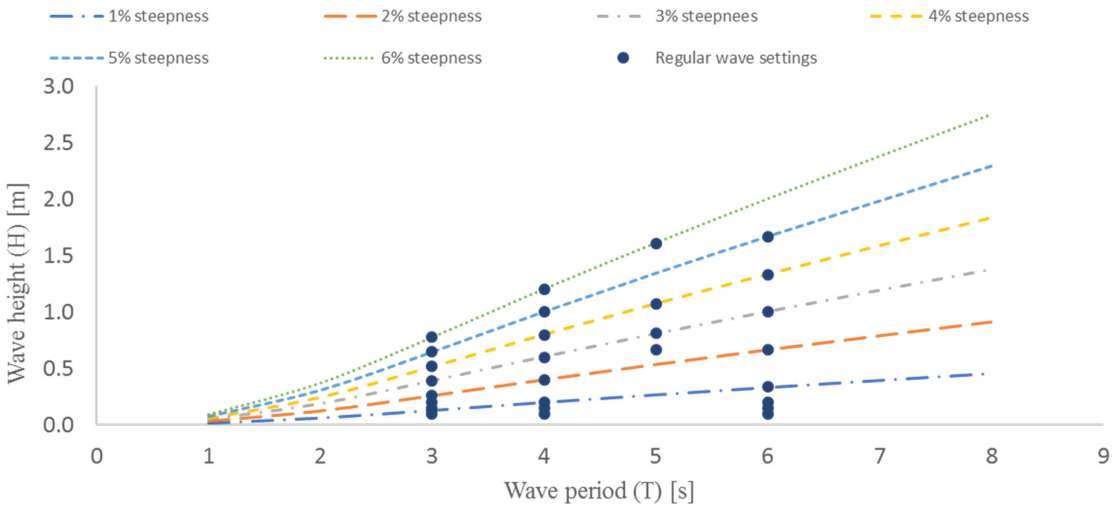

B_c/L	H [m]	Orifice Diameter (A_o/A_c)					
		Closed	0.1%	0.2%	0.88%	0.88% (lowered)	2.00%
0.1394	0.1	/		/		/	
	0.15	/	/	/	/	/	
	0.2	/		/	/	/	
	0.26						
	0.39	/		/	/	/	/
	0.52						
	0.65	/		/		/	/
	0.78						!
0.1045	0.1	/		/	/	/	
	0.15	/	/	/	/	/	
	0.2	/		/		/	
	0.4						
	0.6	/		/		/	/
	0.8				!		!
	1	/	/	/	!	/	/
	1.2	/	/	/	/	/	!
0.0836	0.54				!		!
	0.81	/			!	/	/
	1.07	/	/	/	!	!	!
	1.61	/	/	/	/	/	!
0.0697	0.1	/		/	/	/	
	0.15	/	/	/	/	/	
	0.2	/		/	/	/	
	0.34						
	0.67						^
	1	/	/	/	!	/	/
	1.33	/	/	/	/	/	!

B_c/L_p	H_{m0} [m]	Orifice Diameter (A_o/A_c)					
		Closed	0.1%	0.2%	0.88%	0.88% (lowered)	2.00%
0.1394	0.26						
	0.39	/	/	/		/	/
	0.52		/	/			/
0.1045	0.4	/				/	!
	0.6		/	/			/
	0.8	/	/	/	!	/	/
0.0929	0.26		/	/		/	/
0.0836	0.54				!		!
	0.81	/	/	/	!	/	/
0.0697	0.67		/	/	/		!
	1	/	/	/	!	/	/
0.0643	0.4	/	/	/		/	/